ACS OMEGA

http://pubs.acs.org/journal/acsodf

Article

Synthesis and Biological Evaluation of Novel 1*H*-Benzo[*d*]imidazole Derivatives as Potential Anticancer Agents Targeting Human Topoisomerase I

Stuti Pandey, Pragya Tripathi, Palak Parashar, Vikas Maurya, Md. Zubbair Malik, Raja Singh, Pooja Yadav, and Vibha Tandon*

Cite This: *ACS Omega* 2022, 7, 2861−2880

Read Online

ACCESS | Metrics & More | Article Recommendations | Supporting Information

ABSTRACT: Small molecules that modulate biological functions are targets of modern-day drug discovery efforts. A new series of novel 1*H*-benzo[*d*]imidazoles (BBZs) were designed and synthesized with different functional groups at the phenyl ring and variable lengths of the alkyl chain at the piperazine end as anticancer agents. We identified human topoisomerase I (Hu Topo I) as a probable target of these molecules through a computational study and DNA relaxation assay, a functional assay of the Hu Topo I enzyme. UV absorption, fluorescence, and circular dichroism spectroscopy were used to study interactions between BBZ and DNA. Out of 16 compounds, **11a**, **12a**, and **12b** showed strong binding affinity and thermal stabilization of AT sequence-specific DNA. BBZs were screened against a panel of 60 human cancer cell lines at National Cancer Institute, USA. Most potent molecules **11a**, **12a**, and **12b** showed 50% growth inhibition (GI_{50}) in a concentration range from 0.16 to 3.6 μM cancer cells. Moreover, **12b** showed 50% inhibition of the relaxation of DNA by Hu Topo I at 16 μM. Furthermore, flow cytometry revealed that **11a**, **12a**, and **12b** cause prominent G2M arrest of cancer cells. In view of the above, we propose that **12b** deserves to be further evaluated for its therapeutic use as an anticancer agent.

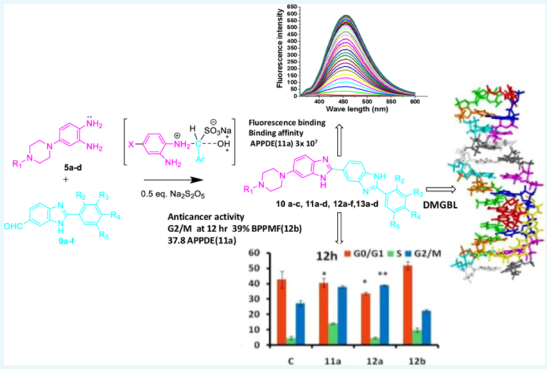

INTRODUCTION

Bisbenzimidazole derivatives have been found to have a variety of biological activities. Bisbenzimidazoles are DNA minor groove-binding ligands (MGBLs) that form non-covalent interactions with the minor groove of DNA and continue to be promising drug candidates in the discovery of potential new anticancer agents.[1−4] Based on the specific mode of binding of MGBL, that is, via hydrogen bonding, electrostatic, and van der Waal's interactions,[5−7] these molecules are used for the treatment of infectious diseases and as chemotherapeutic agents against cancer.[8,9] MGBL's in the majority bind to AT-rich sequences of DNA. These agents are classified according to their interaction through a direct or indirect irreversible interaction with nucleotides causing permanent DNA damage, for example, mitomycin C, anthramycin, CC-1065,[10,11] bleomycins,[12,13] and others that interact only physically with DNA and cause reversible inhibition of DNA-dependent functions such as distamycin A, diarylamidines, DAPI, berenil, pentamidine, and 1*H*-benzo[*d*]imidazoles (BBZs) such as Hoechst-33258, 33342.[14−20] The diverse substitutions at the benzimidazole core gave rise to its antihelmintic,[21,22] antifungal,[23−25] antitumor,[26,27] and antiviral[28] activities. Different substituted benzimidazoles were also evaluated as H2 receptor blockers and proton pump inhibitors.[29] Due to the interference in DNA-mediated enzymatic processes, these BBZ derivatives act through various modes to inhibit the proliferation of cancer cells. The inhibitory activity of DNA topoisomerases advances BBZ to one of the most interesting classes of the therapeutic agent.[30−38] Previously, our group has reported two BBZ analogues,[39] DMA and TBZ (Figure 1), containing disubstituted phenyl ring carrying electron-donating groups such as 3,4-dimethoxy, 3-methoxy 4-hydroxy, and *N*-methyl piperazine at another end. These substitutions resulted in increased lipophilicity and improved sequence specificity that prevent cells from radiation-induced DNA damage. Our previous studies have encouraged us to apply different approaches to correlate the position and identify the terminal substituent of BBZ at the phenyl end and piperazine end, to synthesize new derivatives with enhanced anticancer potency. Different BBZ derivatives were synthesized by substituting electron-withdrawing and

Received: October 14, 2021
Accepted: December 7, 2021
Published: January 10, 2022

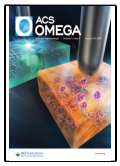

https://doi.org/10.1021/acsomega.1c05743
ACS Omega 2022, 7, 2861−2880

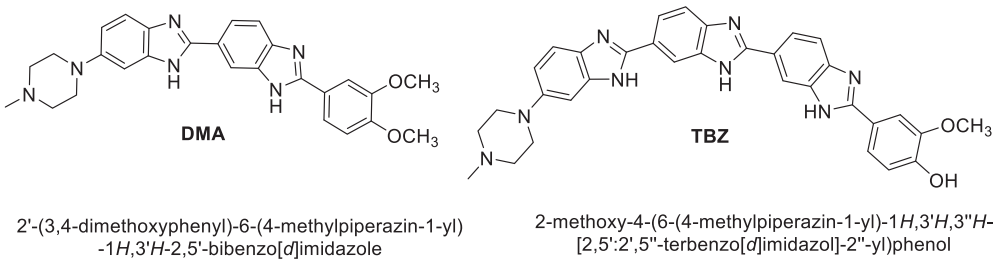

Figure 1. Previously synthesized bisbenzimidazole derivatives.

Scheme 1. Synthesis of *N*-Substituted Piperazin-1-yl Benzene-1,2-diamine Derivatives (5a−d)[a]

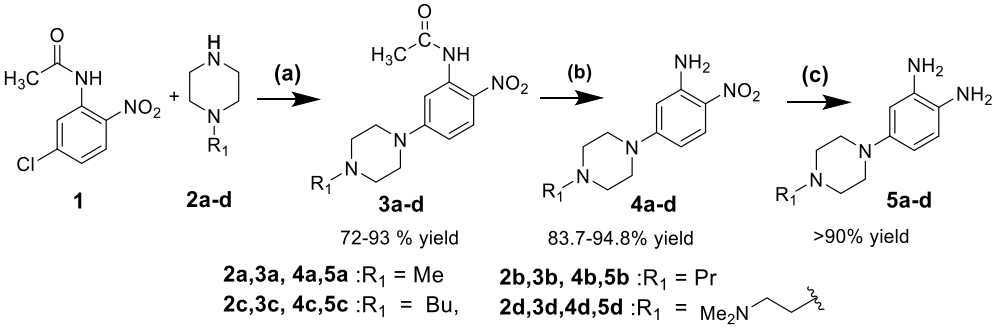

[a]Reaction conditions: (a) **1** (6.98 mmol, l equiv), **2a−d** (8.3 mmol, 1.2 equiv), $(Et)_3N$, (20.94 mmol, 3 equiv), DMSO, 120 °C for 6 h, 72−93%; (b) **3a−d** (3.59 mmol) 10% H_2SO_4, 80 °C for 1.5 h., 83.7−94.8%; and (c) **4a−d** 10% Pd/C, H_2 at 40 psi, EtOAc:MeOH (4:1) 100 mL for 5 h.

Scheme 2. Synthesis of 2-Aryl-5-formylbenzimidazoles (9a−e)[a]

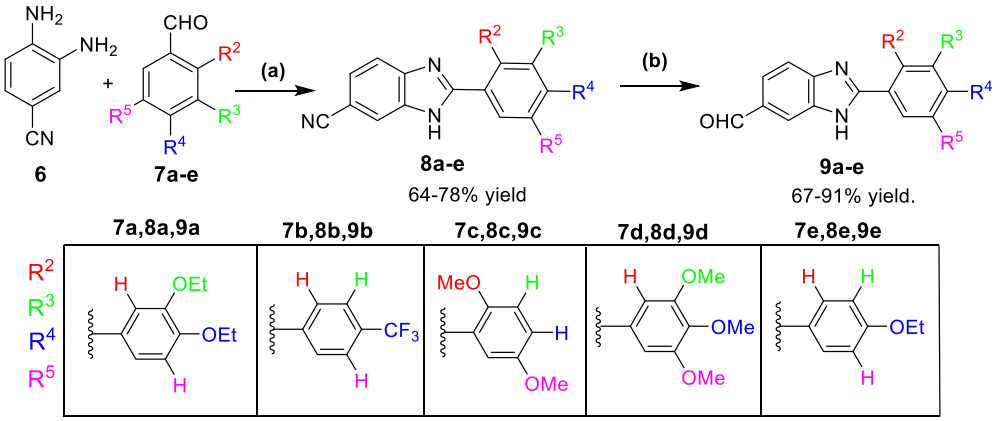

[a]Reaction conditions: (a) **6** (3.75 mmol), **7a−e** (1.5 equiv, 5.6 mmol), $Na_2S_2O_5$ (0.5 equiv, 1.9 mmol) in 2.5 mL of water, ethanol, reflux for 4−6 h, 64−78% isolated yield; (b) **8a−e** (2.6 mmol), Ni−Al alloy (0.036 mmol 1.2 eqiuv), 75% HCOOH, 95 °C, 3 h, 67−91% isolated yield.

electron-donating groups at the phenyl end and insertion of different lengths of the carbon chain at the N1 position of piperazine with propyl, butyl, and *N*,*N*-dimethylaminoethyl chains. Previous studies on MGBL by spectroscopic techniques identified sequence-specific binding of the molecules to the minor groove of DNA.[40−44]

In addition, we have performed a molecular docking study to correlate our findings with a theoretical approach. We have also investigated the binding affinity of the BBZ derivatives with B-DNA using UV−vis, thermal denaturation, fluorescence, and circular dichroism (CD) spectroscopic techniques. The synthesized BBZ derivatives were evaluated for the anticancer potential at the National Cancer Institute (NCI), USA, against a panel of NCI 60 cell lines.[45−50] Out of all molecules, **11a**, **12a**, and **12b** were observed to be most potent molecules with the lowest 50% growth inhibition (GI_{50}) values against 60 different cancer cell lines. Compound **12b** inhibited human topoisomerase I (Hu Topo I) enzyme at 16 μM (IC_{50}) concentration, which was comparable to IC_{50} of camptothecin (CPT) in our assay. Furthermore, flow cytometric studies provided evidence that **11a**, **12a**, and **12b** cause the G2/M phase of the cell cycle arrest. Cell cycle arrest at the G2/M phase indicates that the DNA damage is challenging to be repaired.

RESULTS AND DISCUSSION

Chemistry. The previously reported methodology for the synthesis of benzimidazole includes the condensation of *o*-phenylenediamine with carboxylic acid under harsh dehydrating reaction conditions such as hydrochloric acid, *p*-toluenesulfonic acid, boric acid, and polyphosphoric acid.[51−53] Similarly, another methodology involving condensation of *o*-phenylenediamine with aldehydes in the presence of oxidizing agents such as

https://doi.org/10.1021/acsomega.1c05743
ACS Omega 2022, 7, 2861−2880

Scheme 3. Synthesis of BBZ Compounds (10a−c, 11a−d, 12a−e, and 13a−d)[a]

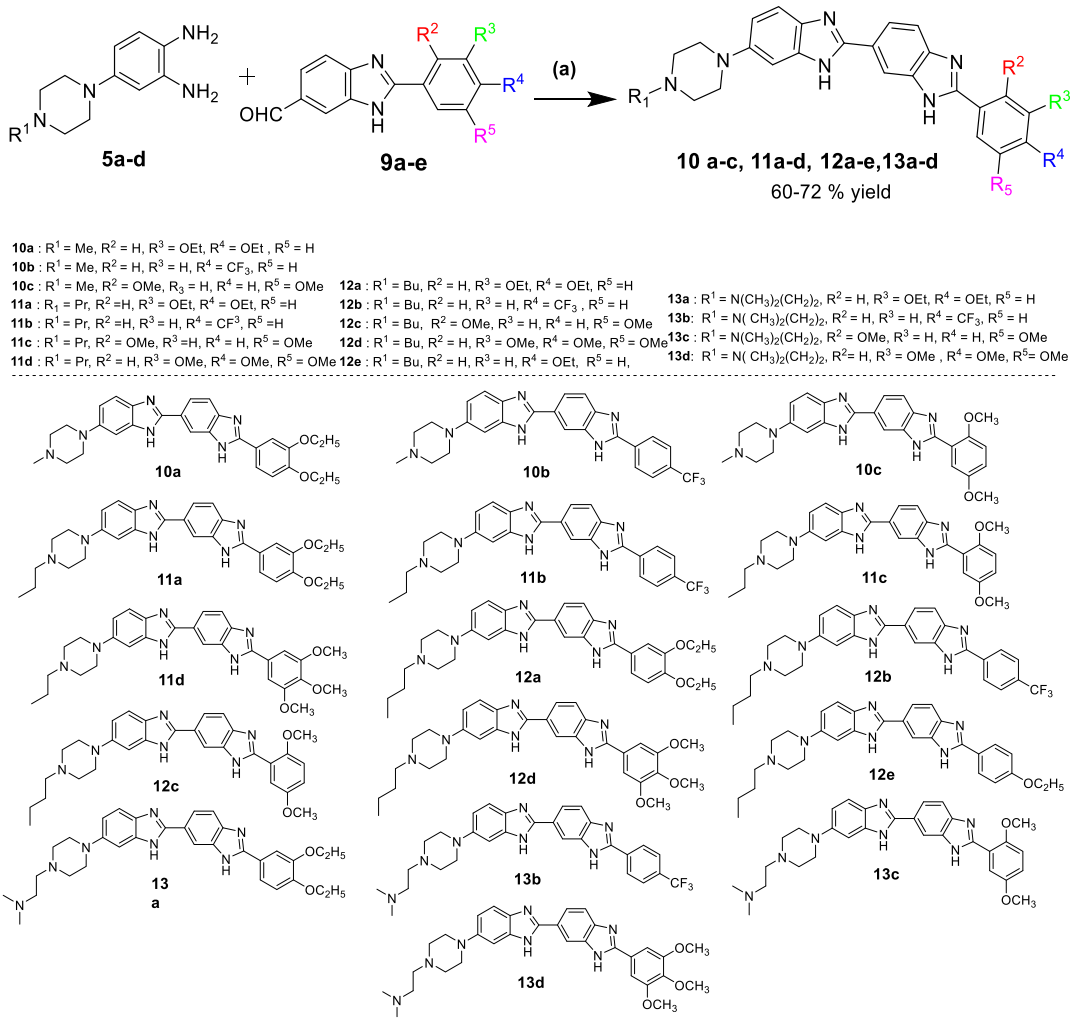

[a]Reaction conditions: (a) **5a−d** (1.46 mmol, 1 equiv), **9a−e** (2.2 mmol, 1.5 equiv), $Na_2S_2O_5$ (0.73 mmol, 0.5 equiv) in 1 mL of water, ethanol, reflux for 24 h, 60−72% isolated yield. The structures of all the synthesized final molecules are mentioned here.

benzoquinone, copper(II) acetate, indium perfluorooctanesulfonates, mercuric oxide, nitrobenzene, lead tetra-acetate, iodine, and even air has been reported in the literature.[54−58] We have used sodium metabisulfite ($Na_2S_2O_5$) as an oxidizing agent, and condensation was carried out in ethanol to synthesize novel bis-benzimidazoles.[59] The electronic effects of the variably substituted aldehydes, both with electron-withdrawing groups (trifluoromethyl) and electron-donating groups (dimethoxy, diethoxy, trimethoxy), have been investigated for the anticancer property.

The synthesis procedure for the preparation of target bisbenzimidazole compounds and their intermediates is shown in Schemes 1−3. BBZ derivatives, **10a−c**, **11a−d**, **12a−e**, and **13a−d**, were synthesized, as per the reported method[59] (Scheme 3). The scheme for the first diamine intermediates is a multi-step process involving reactions like acetylation, deacetylation, hydrogenation, and so forth (Scheme 1). The diamine intermediates, **5a−d**, were prepared by a nucleophilic substitution reaction of 5-chloro-2-nitroacetanilide **1** (1.46 mmol) with the N-substituted piperazines (1.5 equiv), **2a−d**, in the presence of triethylamine (TEA, 3 equiv) in DMSO with stirring at 120 °C to produce 2-nitroacetanilide derivatives **3a−d** with the 71.7−98% yield. Deacetylation of **3a−d** was carried out using 10% sulfuric acid to obtain **4a−d** with excellent yields. The deacetylated intermediates, **4a−d**, were reduced by catalytic hydrogenation using 10% Pd/C at 40 psi at rt to obtain diamine derivatives, **5a−d**, in >90% yield (Scheme 1).

Second intermediates, 2-aryl-5-cyano-1*H*-benzimidazoles, **8a−e**, were synthesized by reacting 4-cyano-1,2-phenylenediamine **6** (3.75 mmol) with the appropriately substituted benzaldehydes, **7a−e**, using the reported method (Scheme 2).[59] Catalytic reduction of **8a−e** by Ni−Al alloy in the presence of 75% formic acid in the water provides intermediates 2-aryl-5-formyl-1*H*-benzimidazole **9a−e**, with the 67−91% quantitative yield (Scheme 2).

Condensation of two intermediates, 4-piperazinyl-phenylenediamine derivatives, **5a−d**, (1.46 mmol 1 equiv), and aldehydes require **9a−e** (2.2 mmol, 1.2 equiv) in $Na_2S_2O_5$ in the ethanol solvent. The oxidizing agent $Na_2S_2O_5$ forms sodium bisulfite ($NaHSO_3$) in water which then forms an adduct with aldehyde and reacts with the diamine derivatives to give the final compounds viz; **10a−c**, **11a−d**, **12a−e**, and **13a−d** in 62−72% isolated yield (Scheme 3). All the final compounds and intermediates were confirmed through ^{1}H NMR, ^{13}C NMR (Figures S1−S52), and MS/HRMS (Figures S53−S69). To increase the water solubility of all the newly synthesized

https://doi.org/10.1021/acsomega.1c05743
ACS Omega 2022, 7, 2861−2880

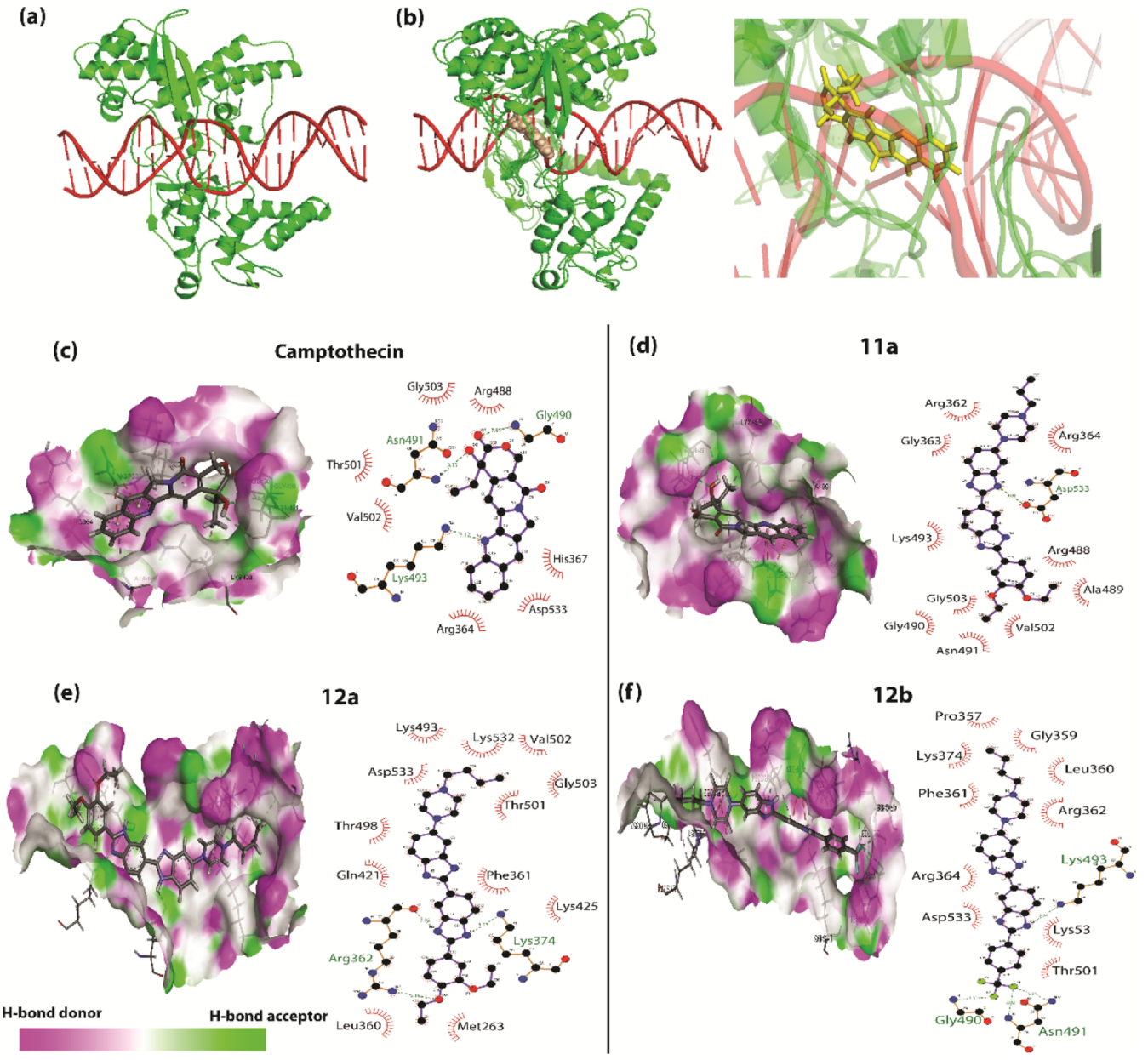

Figure 2. Molecular docking interactions and orientations of CPT, **11a**, **12a**, and **12b** and with Hu Topo I enzyme: DNA complex using Glide and construction of the 2D and 3D model through Ligplots and BIOVIA discovery studio. (a) Structure of the Hu Topo I DNA complex without CPT. (b) Structure of the Hu Topo I DNA complex with CPT. The binary complex is diagrammed with protein (green) and DNA (red). The 2D docking interactions of Hu Topo I with compound (c) CPT, (d) **11a**, (e) **12a**, and (f) **12b**. The right panel shows a schematic representation of interactions made by these BBZs with Hu Topo I. H bond and hydrophobic analysis of docking poses were carried out using Ligplots (blue line—ligand bonds; red line non-ligand bonds; dotted lines—hydrogen bonds and its length; half red circle non-ligand residues involved in the hydrophobic contacts; and black dots—corresponding atoms involved in the hydrophobic contacts).

Table 1. Binding Affinities of the Given Compounds with Human Topoisomerase I: DNA Complex

ligands	Glide score (kcal/mol)	hydrogen bonding	hydrophobic interaction
camptothecin	−6.001	Gly490, Asn491, Lys493	His367, Arg364, Arg488, Thr501, Val502, Gly503, Asp533
11a	−5.453	Asp533	Arg362, Gly363, Arg364, Arg488, Ala489, Gly490, Asn491, Lys493, Val502, Gly503
12a	−5.429	Arg362, Lys374	Met263, Leu360, Phe361, Gln421, Lys425 Kys493, Thr498, Thr501, Val502, Gly503, Lys532, Asp533,
12b	−5.512	Gly490, Asn491, Lys493	Pro357, Phe361, Atg364, Pro357, Gly359, Lys374, Thr501, Lys532, Leu360, Arg362, Asp533

benzimidazole derivatives, the compounds were further converted to their respective hydrochloride salts by passing dry HCl gas into a methanolic solution.

Molecular Docking Study of Ligands with Human Topoisomerase I (Hu-TopoI) DNA Complex. Molecular docking studies helped us in better understanding the binding

https://doi.org/10.1021/acsomega.1c05743
ACS Omega 2022, 7, 2861−2880

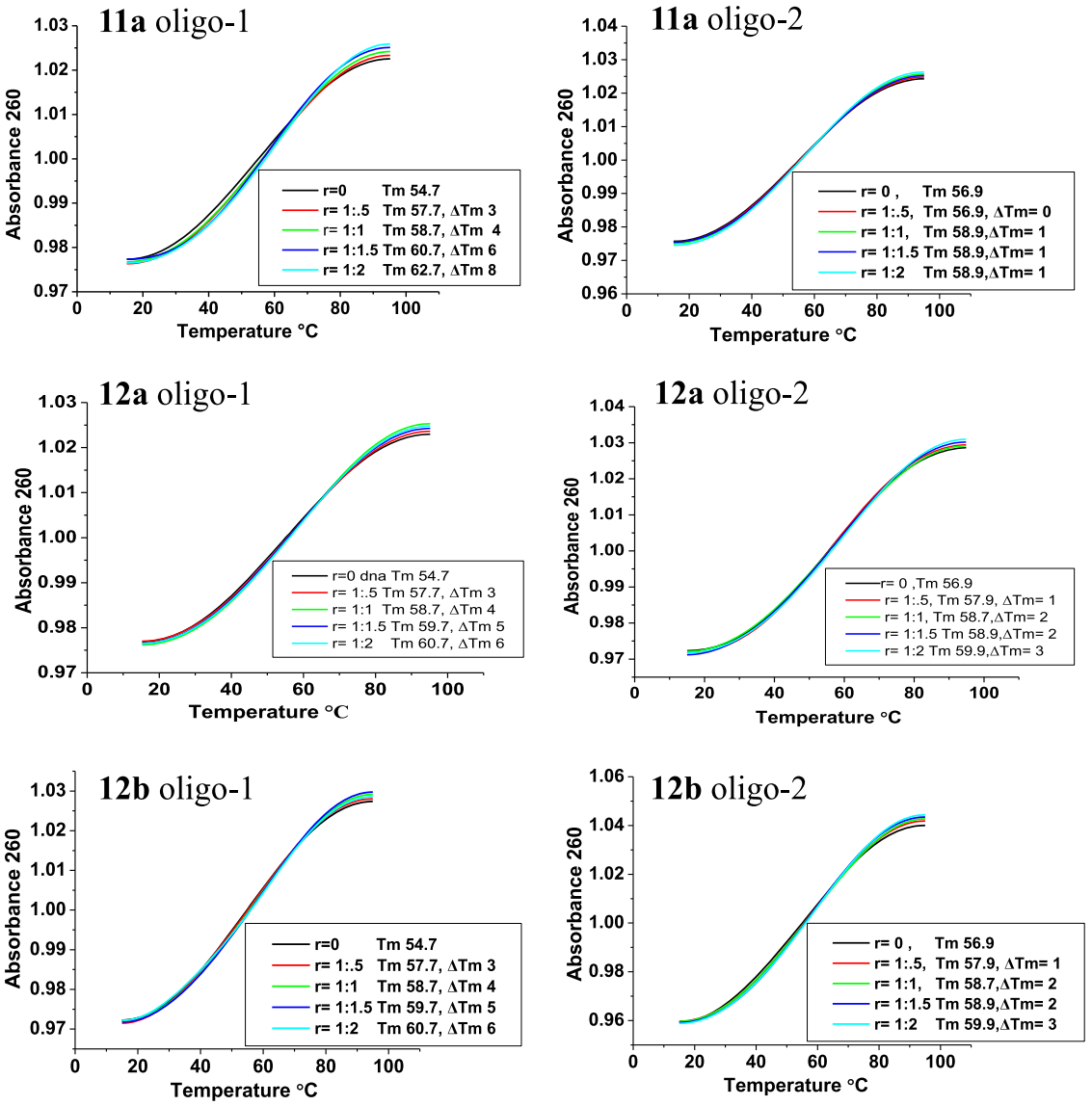

Figure 3. Distinct UV melting profiles of oligomer-1 and 2, i.e., d(CGCGAATTCGCG)$_2$ and d(CGATGTACATCG)$_2$ alone and in the presence of ligands **11a**, **12a**, and **12b** at a ligand/oligomer ratio, r = 0−2. Samples of DNA (2.5 μM) were mixed with ligand (1.25−5 μM) in buffer [20 mM sodium cacodylate, 100 mM NaCl (pH 7.2)] before being heated at 95 °C for 5 min and slowly annealed to 4 °C before UV analysis at 260 nm from 15 to 95 °C at a heating rate of 0.2 °C/min. T_m values were determined by first-derivative analysis.

interactions of synthesized active compounds within the Hu Topo I DNA complex (Figure 2a,b). The molecular docking of the compounds **11a**, **12a**, and **12b** was performed with Hu Topo I DNA complex (PDB entry 1EJ9)[60] (https://www.rcsb.org) and compared with CPT, a standard Hu Topo I inhibitor. Molecular docking was carried out using Glide.[61] The analysis of the X-ray crystal structure of Hu Topo I covalently joined to double-stranded DNA and bound to the anticancer agent topotecan (a synthetic analogue of CPT) suggests that topotecan binds at the site of DNA cleavage by intercalating between the upstream (−1) and downstream (+1) DNA base pairs. Intercalation displaces the downstream DNA, thus preventing relegation of the cleaved strand. Topotecan acts as an uncompetitive inhibitor by specifically binding to the enzyme−substrate complex.[63] The 2D and 3D models of the ternary complex BBZs:DNA:Hu Topo I were constructed through Ligplots+[64] and BIOVIA discovery studio[65] (Table 1). The CPT displayed the strong hydrogen bonding with Gly490, Asn491, and Lys493 at a distance of 2.95, 3.25, and 312 Å, respectively, and van der Waals interactions with His367, Arg364, Arg488, Thr501, Val502, Gly503, and Asp533 (Figure 2c). The binding affinities of the compounds were as **11a** (−5.453 kcal/mol), **12a** (−5.429 kcal/mol), and **12b** (−5.512 kcal/mol). The **11a** displayed H-bonds with Asp533 at a distance of 3.01 Å along with the hydrophobic and van der Waals interactions with residues like Arg362, Gly363, Arg364, Arg488, Ala489, Gly490, Asn491, Lys493, Val502, and Gly503 (Figure 2d). Besides, **12a** interacts with Hu Topo I with H-bonds involving Arg362 and Lys374 along with hydrophobic and van der Waal interactions with Met263, Leu360, Phe361, Gln421, Lys425, Kys493, Thr498, Thr501, Val502, Gly503, Lys532, and Asp533, displaying the strong affinity (Figure 2e). **12b** interacts with Hu Topo I through hydrogen bonds with Gly490 and Lys493 along with hydrophobic and other van der Waal interactions mediated by Pro357, Phe361, Atg364, Pro357, Gly359, Lys374, Thr501, Lys532, Leu360, Arg362, and Asp533

https://doi.org/10.1021/acsomega.1c05743
ACS Omega 2022, 7, 2861−2880

Table 2. T_m (°C) of Synthetic Duplex Oligo-1: d(CGCGAATTCGCG)$_2$ and Oligo-2: d(CGATGTACATCG)$_2$ with All Ligands (r = Ligand/DNA)[a]

	r = 0	r = 0.5		r = 1		r = 1.5		r = 2.0	
study system	T_m	T_m	ΔT_m	T_m	ΔT_m	T_m	ΔT_m	T_m	ΔT_m
oligo-1 + **11a**	54.7	57.7	3	58.7	4	60.7	6	62.7	8
oligo-2 + **11a**	56.9	57.9	1	58.9	2	58.9	2	5.9	2
oligo-1 + **12a**	54.7	56.7	2	57.7	3	58.7	4	61.7	7
oligo-2 + **12a**	56.9	57.9	1	58.9	2	58.9	2	59.9	3
oligo-1 + **12b**	54.7	57.7	3	58.7	4	59.7	5	61.7	7
oligo-2 + **12b**	56.9	57.9	1	58.9	2	58.9	2	59.9	3

[a]UV/vis absorption studies.

(Figure 2, **11b**). The compounds **11a**, **12a**, and **12b** showed considerably good binding affinity to Hu Topo I and interacts through H bonds, hydrophobic interactions, and van der Waals interactions (Figure 2d−f). Since approximately equal number of poses and similar energies were obtained for compounds **11a**, **12a**, and **12b**, the conformations were kept for further analysis.

Rationale for Choice of Oligonucleotides. The interaction of all BBZ analogs (Scheme 2) with DNA has been studied by biophysical techniques. The X-ray crystal structure study of the complex of Hoechst 33258 and the DNA dodecamer CGCG-AATTCGCG suggests that Hoechst 33258 is located in the narrow central AATT region of the minor groove.[66,67] Earlier studies suggested that at 25 and 100 °C, the Hoechst 33258/DNA binding ratio (r) is 1:1, whereas this ratio changed to 2:1 at 0 °C. The dihedral angles between the rings of Hoechst 33258 appear to change in a temperature-dependent manner. Thus, we have selected two oligonucleotides, oligo-1: d(CGCGAATTCGCG)$_2$ and oligo-2: d-(CGATGTACATCG)$_2$ for our study.[68−70]

Determination of the Ligand-DNA UV Melting Profile. We performed thermal denaturation experiments of oligo-1 {d(CGCGAATTCGCG)$_2$} and oligo-2 {d-(CGATGTACATCG)$_2$} (2.5 μM) with and without BBZs. All 16 BBZ derivatives (Figure 3) showed binding with both the oligos (Tables 2 and S1). BBZs had a higher affinity of binding with oligo-1 as compared to oligo-2. The **10a−b**, **11a−d**, **12a−e**, and **13a−13c** showed ΔT_m in the range 1 to 5 °C with oligo-1 at a BBZ/oligomer ratio, r = 0.5 (Table 2). When we increased the BBZ/oligomer ratio, r = 2, ΔT_m value also increased and was observed in the range of 5 to 9 °C. The **10c** and **13d** displayed no significant improvement in ΔT_m at r = 1.5 or 2 with both the oligonucleotides (Table 2). Throughout duplex formation, the sigmoid curves were observed as a new distinct peak as the first derivative of all BBZs and proved to be minor groove binders without any deformation. These results suggest that the longer alkylated chain at the piperazine end along with the mono- and disubstituted phenyl ring of the BBZ moiety increases its binding in the minor groove of oligo-1. However, *N*,*N*-di-methyl aminoethyl alkyl chain inserted at the piperazine end and trisubstitution on the phenyl ring was observed to be an unfavorable modification in the compounds (**11d**, **12d**, **13a**, **13c**, and **13d**) for binding affinity with oligo-1. With oligo-2, **10a−b**, **11a−d**, **12a−b**, **12d−e**, and **13b** showed maximum change in melting temperatures, ΔT_m = 3 and 4 °C at r = 0.5 to 2. However, the **10c**, **12c**, and **13b−d** showed no such gradual increase in melting temperature with an increase in the ratio from r = 0.5 to 2. The variations between the two sequences in melting temperature are visible with distinct melting patterns (Figures 3 and S69−S72 and Table S1), which suggest that how bisbenzimidazoles recognize the different sequences of DNA differentially. This proves that BBZs can differentiate between the different conformations of DNA.

UV/Vis Absorption Studies. All the BBZs exhibit absorption maxima between 347 and 355 nm. To assess the sequence specificity, the binding of the BBZs with specific AT sequence and GC mixed oligomer was studied by calorimetric methods at a fixed ligand/oligomer ratio, r = 1. There was a progressive increase in absorption intensity, and a continued red shift was observed in absorption spectra with decreasing BBZ/DNA ratio. A significant red shift of 18 nm was observed with **12b** after binding to oligo-1. Hoechst-33342 exhibits an 18 nm of redshift with oligo-1, which was the same as that to **12b** (Table 3), suggesting that the **12b** has higher specificity for AT-rich DNA. The absorption maxima for **10a**, **11a**, **11b**, **12a**, and **12e** showed a redshift of 14, 15, 16, 16, 16 nm, respectively, at BBZ/DNA ratio, r = 1.0. With GC mix oligo-2, **10a**, **11b**, **12a**, **12e**, **13a**, and **13b** showed the redshift in the range of 9−12 nm (Table 3), and Hoechst-33342 showed a redshift of 9 nm, which was comparatively similar to the synthesized BBZ. A higher red shift observed with these ligands can be correlated to random binding with oligo-2 (Figures S73 and S74). The hypochromicity/hyperchromicity in the absorption spectra is mostly

Table 3. Binding Affinity Obtained from Fluorescence Titration Experiments and Red-Shift Observed from UV−Visible Titration of Oligo−Ligand Complexes

	K_a		K_a	
BBZs	binding affinity with oligo-1 (M^{-1})	UV titration redshift (nm)	binding affinity with oligo-2 (M^1)	UV titration redshift (nm)
10a	7×10^6	14	2×10^6	10
10b	7×10^6	10	3×10^6	8
10c	8×10^6	11	2×10^6	8
11a	3×10^7	15	5×10^6	8
11b	7×10^6	16	2×10^6	10
11c	7×10^6	8	3×10^6	2
11d	8×106	12	1×10^6	5
12a	1×10^7	16	4×10^6	10
12b	1×10^7	18	2×10^6	9
12c	6×10^6	9	2×10^6	3
12d	9×10^6	13	4×10^6	5
12e	1×10^7	16	3×10^6	6
13a	9×10^6	12	2×10^6	12
13b	7×10^6	12	2×10^6	9
13c	5×10^6	7	1×10^6	3
13d	5×10^6	11	1×10^6	4
H 33342	2×10^7	18	5×10^6	12

https://doi.org/10.1021/acsomega.1c05743
ACS Omega 2022, 7, 2861−2880

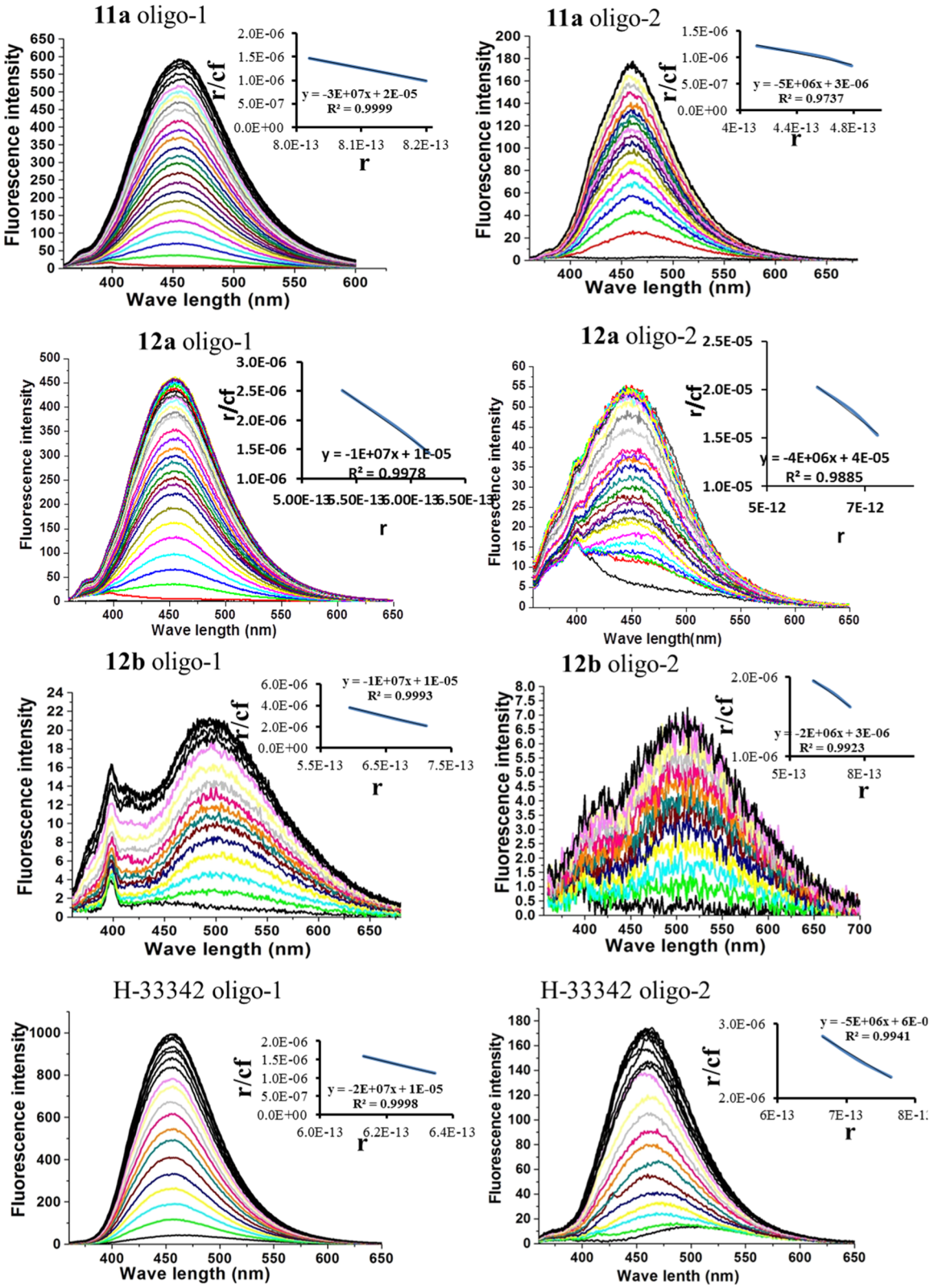

Figure 4. Fluorescence titration binding study of oligo-1: d(CGCGAATTCGCG)$_2$ and oligo-2: d(CGATGTACATCG)$_2$ with ligands (**11a**, **12a**, and **12b**). 1−20 μL of oligos (stock 0.1 mM) were added to a solution of ligand (1 mL of a 1 mM solution), and emission scanning was carried out from 360 to 680 at 2 nm/s speed; 5 nm slit width; T = 20 °C in a buffer containing 20 mM sodium cacodylate (pH 7.2) and 100 mM Na.

attributed to the interaction between the electronic states of the ligand chromophore and those of the DNA bases. On the other hand, the red shift is associated with a decrease in the energy gap between the highest and lowest occupied molecular orbits when the ligand binds to DNA. The extent of the red shift follows the order d(CGATGTACATCG)$_2$ < d(CGCGAATTCGCG)$_2$ in the case of all synthesized BBZs and suggests that BBZ binds in a non-cooperative manner with no differential recognition of

https://doi.org/10.1021/acsomega.1c05743
ACS Omega 2022, 7, 2861−2880

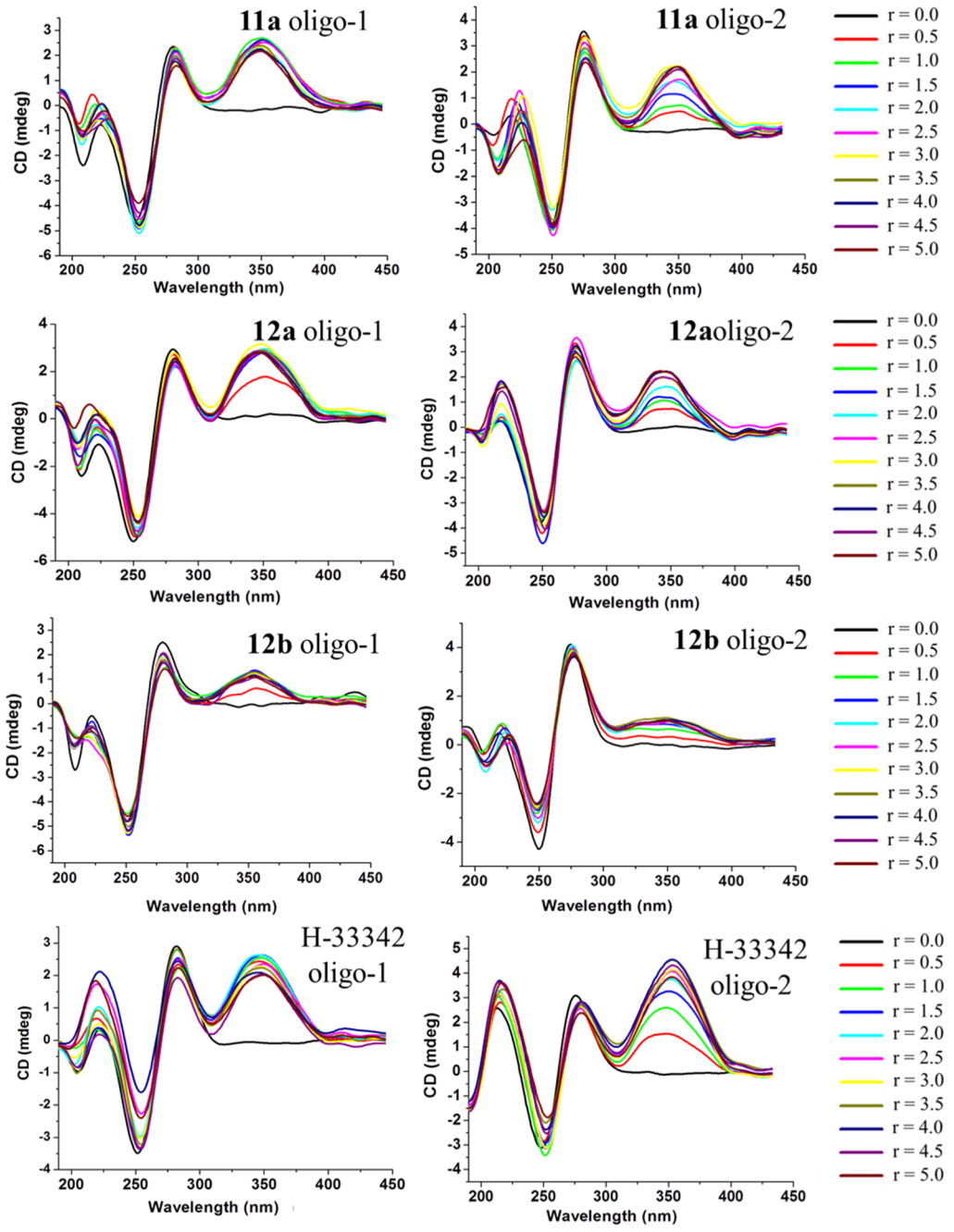

Figure 5. CD scans of oligomer-1 and oligomer-2, i.e., d(CGCGAATTCGCG)$_2$ and d(CGATGTACATCG)$_2$ with increasing concentrations of ligands (**11a**, **12a**, **12b**, and Hoechst 33342) at 20 °C. Samples of the oligomer (10 μM) were scanned from 450 to 190 nm after serial additions of the concentrated ligand with stirring. Peaks around 347−352 nm correspond to the ligand−oligomer complex. Buffer: 20 mM sodium cacodylate, 100 mM NaCl (pH 7.2); *r* stands for the ligand/oligomer ratio.

mixed DNA due to the substitution of bulky ethoxy and methoxy groups at ortho, meta, and para positions, respectively.

Fluorescence Spectroscopy Studies. The fluorescence spectrum of free ligands from **10a−10c**, **11a−11d**, **12a−12e**, and **13b−13d** contains a single broad emission band from 410 to 560 nm. BBZ analogs, the 2, 5 di-methoxy and CF_3-substituted BBZs viz. **10c**, **11c**, **12c**, **13c**, **10b**, **11b**, **12b**, **13b**, and **13c**, have comparatively weak fluorescence intensity. **11d**, **12d**, **11a**, **12a**, **12e**, and **13a** displayed moderate and strong fluorescence intensity. In fluorescence titration, most BBZs showed a blue shift of 20−35 nm, while Hoechst 33342 showed a blue shift of 20 nm with oligo-1. For oligo-2, the minimum value of the blueshift change was 2−3 nm with the synthesized BBZ, while Hoechst 33342 showed a blueshift of 15 nm with oligo-2. The fluorescence of **11a**, **12a**, and **12b** upon binding with oligo-1 has increased significantly compared to oligo-2 at a BBZ/oligomer ratio, $r = 2$.

Further evaluation of their binding strength with oligomeric duplex demonstrated the strong binding affinity for **11a** ($K = 3 \times 10^7$), **12a** ($K = 1 \times 10^7$), **12b** ($K = 1 \times 10^7$), and Hoechst 33342 ($K = 2 \times 10^7$) with the oligo-1. The obtained binding affinity values confirm the increased sequence selective binding by these BBZs (Table 3). However with oligo-2, relative fluorescence enhancement after BBZ complexation was comparatively less

https://doi.org/10.1021/acsomega.1c05743
ACS Omega 2022, 7, 2861−2880

Table 4. Calculated Values of GI_{50}, TGI, and LC_{50} (in μM) of the Selected BBZs against NCI Cell Line Panels

	12b			11a			12a		
60 cancer cell lines	GI_{50}	TGI	LC_{50}	GI_{50}	TGI	LC_{50}	GI_{50}	TGI	LC_{50}
Leukemia									
CCRF-CEM	0.3	1.03	5.04	0.4	3.6	>100	0.53	3.06	>100
HL-60(TB)	1.2	2.8	6.6	0.37	2.7	>100	0.70	3.18	67.9
K-562	0.22		>100	0.31	1.5		0.52	2.27	7.53
MOLT-4	1.07	2.5	6.3	0.59	4.4	>100	1.22	3.86	31.6
RPMI-8226	0.25	0.62		0.47	2.5	>100	0.43	2.06	>100
SR	0.26	0.65		0.29		>100	0.31	1.19	>100
Non-Small Cell Lung									
A549/ATCC	0.35	1.19		1.17	3.02		1.18	2.93	
EKVX	1.5	2.9	5.7	1.73	13.3	>100	1.38	3.18	
HOP-62	1.3	3.05		1.98	5.2	23.4	1.81	3.40	
HOP-92	1.18	2.78	6.5	1.2	4.5	26.3	1.23	3.17	8.15
NCI−H226	1.57	3.59		0.8	3.5	37.5	1.29	3.95	>100
NCI−H23	1.65	3.36	6.8	0.25	0.7	4.24	0.78	2.35	
NCI−H23M	1.39	2.74	5.39	1.1	3.2	9.18	1.27	2.67	5.65
NCI−H460	0.23	0.5	1.62	0.43	1.51	4.38	0.53	1.86	5.31
NCI−H522	1.6	3.6		0.45	2.11		1.20	3.97	>100
Colon Cancer									
COLO 205	1.3	3.1		0.16	1.29	5.4	0.23	1.52	6.18
HCC-2998	1.8	3.5	6.6	1.24	2.62	5.5	1.71	3.22	
HCT-116	0.2	0.42		0.24	1.23	4.7	0.43	1.66	4.30
HCT-15	0.27	0.74		2.42	18.9	>100	1.56	3.32	7.05
HT29	0.34	1.42		0.45	2.3	>100	0.80	2.97	100
KM12	0.67	2.04	4.9	1.26	2.8	6.4	1.42	2.99	6.28
SW620	0.21	0.45	0.45	0.30	1.2	4.3	0.47	1.79	5.15
CNS									
SF-268	1.7	3.3	6.4	1.9	11.5	68.8	2.66	22.0	>100
SF-265	1.34	2.7	5.4	0.5	2.3	7.8	0.70	2.26	
SF-539	1.6	3.05	5.8	0.79	2.1	4.8	1.26	2.56	5.20
SNB-19					2.18	5.6	1.22	2.61	5.58
SNB-75	1.05	2.25	4.8	0.71	1.9	4.3	0.65	2.01	4.54
U251	0.24	0.56		0.42	1.8	4.8	1.28	2.69	5.65
Melanoma									
LOX IMVI	0.38	1.1		0.2	0.44	0.96	0.42	1.62	
MALME-3M	1.4	3.0		0.08	1.2	3.9	0.19	1.18	
M14	0.37	2.4		0.25	1.5	5	0.31	1.55	4.68
MDA-MB-435	1.4	2.8	5.5	0.67	1.9	4.5	1.09	2.39	5.24
SK-MEL-2	1.8	3.3	6.3	14	3.1		1.68	3.66	
SK-MEL-28	1.7	3.1	5.9	0.91	2.2	5.2	1.01	2.22	4.86
SK-MEL-5	1.6	3.2	6.2	0.63	2.01	4.6	1.09	3.16	9.22
UACC-257	1.7	3.5	7.2	0.79	2.8	9.4	1.21	10.5	>100
UACC-62	1.5	2.9	5.8	0.4	1.9	5.3	0.68	2.18	5.42
Ovarian									
IGROV1	1.7	3.4		0.76	4.1	37.8	1.15	2.60	.
OVCAR-3	0.21	0.4	0.73	0.26	0.58	1.8	0.35	0.85	2.92
OVCAR-4	0.6	1.8	5.2	0.69	2.8	9.5	1.48	3.21	6.95
OVCAR-5	1.8	3.5	5.9	2.09	5.01	15.9	1.90	3.40	6.08
OVCAR-8	1.1	2.8		0.45	2.16	>100	0.89	3.06	
NCI/ADR-RES	2.1	57.7	>100	>100	>100	>100	100	100	>100
SK-OV-3				2.1	10.2	9.9	1.33	3.27	8.01
Renal									
786−0	1.47	3.04		1.13	2.50	5.54	1.41	2.84	5.72
A498	1.69	3.31	6.49	0.47	1.79	4.38	1.18	2.47	5.16
ACHN	1.32	2.6	5.14	0.82	2.1	4.77	0.92	2.12	4.65
CAKI-1	1.29	2.58	5.15	1.04	3.03	8.8	1.04	2.52	6.12
RXF393	0.47	1.5		0.26	0.9	3.6	1.01	2.35	.
SN12c	1.54	3.02		0.45	2.06	6.75	1.03	2.61	.
TK-10				1.22	4.9	2.47	1.66	5.17	>100
UO-31	1.77	3.24	5.9	1.67	3.82	8.76	2.00	5.80	43.8

https://doi.org/10.1021/acsomega.1c05743
ACS Omega 2022, 7, 2861−2880

Table 4. continued

60 cancer cell lines	12b			11a			12a		
	GI_{50}	TGI	LC_{50}	GI_{50}	TGI	LC_{50}	GI_{50}	TGI	LC_{50}
Prostate									
PC-3	0.86	2.31	5.5	0.38	1.92	6.12	1.08	2.44	5.49
DU-145	0.45	1.68	4.3	0.44	2.02	12.4	1.00	2.21	4.88
Breast									
MCF7	0.17	0.57		0.35	1.53		0.19	1.42	
MDA-MB-231	1.46	2.92	5.84	1.38	3.06	6.78	1.69	3.28	6.38
HS578T	1.26	3.05 -	1.09	3.68	>100		1.54	3.90	
BT-549	1.62	3.15		1.22	2.72	6.07	1.55	3.07	
T-47D	1.24	3.23		0.91	9.11	>100	1.36	7.88	>100
MDA-MB-468	1.66	3.34		0.43	1.82	7.07	1.27	3.09	

than the oligo-1 (Figure 4). The results indicate that the BBZ analogs **11a**, **12a**, and **12b**, including Hoechst 33342, have a strong affinity with the oligo-1 sequence, where more AT bases are located in the minor groove. It was also shown that the ligand binding to DNA was AT sequence-specific rather than random mix sequences (Figure 4). The fluorescence spectra of other molecules are given in the Supporting Information. The binding affinity was calculated from the Scatchard plots (r/C_f vs r) and fitted to data (Figures S75 and S76). Based on the obtained results, it can be suggested that selectivity was established for minor groove-oriented BBZs due to the following reason: (a) B-DNA's electrostatic potential is most negative in the AT-rich region of the minor groove and thus facilitates the binding of cationic drugs and (b) the small groove width is narrower in the AT region, thereby stabilizing the desired bound molecule through the desirable van der Waals interactions. The results indicate that BBZ analogs with 3,4-diethoxy, 4-ethoxy (**11a**, **12a**, and **12b**) substituted at the phenyl end act as strong binders relative to the multiple substitutions at the phenyl ring. Apart from this, it is also reported that the NH group of the imidazole ring has strong H-bond interaction with the nucleic acid base in DNA. Hence, an increase in electron density at N-atom upon substitution with an electron-donating group at the phenyl end increases the feasibility and strength of H-bond formation between NH-imidazole and electronegative "O"-atoms of nucleic acid bases. However, compound **12b**, having a strong electron-withdrawing group, CF_3, at the phenyl ring end, also showed strong binding to oligo-1. Piperazine itself and three to four carbon long side chains on piperazine favor the binding of BBZs in the minor groove with a specific AT sequence. From overall observations, we found that bi/mono substitution at the phenyl end and chain lengthening at the piperazine end of BBZ analogs (**10a**, **11a**, **11b**, **12a**, **12b**, and **12e**) enable them to interact more firmly with both DNA sequences as compared to other bulkier analogs like tri-methoxy substitutions at the phenyl ring and *N*,*N*-dimethylaminoethyl alkylating chain substituted at the piperazine end of BBZ.

Circular Dichroism Studies. CD titration is an effective method of evaluating the binding mode and the saturation limit for BBZ binding with oligos. The conformation of DNA is influenced by the binding of the compounds to DNA. The changes in CD signals were observed upon the interaction of DNA with compounds which may often be assigned to the corresponding changes in the DNA structure. Neither oligo-1 and oligo 2 nor the ligands (**11a**, **12a**, **12b**, and Hoechst 33342) alone exhibited CD signals, but the asymmetry in the optical properties of the ligands due to the effect of the DNA field results in differentially induced CD spectra of the complexes at 340−360 nm. The CD spectroscopic studies were carried out with three molecules, **11a**, **12a**, **12b**, and Hoechst 33342 (as control) complexes with each of the oligo 1 and oligo 2 as these molecules exhibit potent anticancer activity in *in vitro* studies. These BBZ showed an induced cotton effect due to the complexation with oligo-1 at different wavelengths, but peak intensity was centered at around 340−360 nm (Figure 5) with varying shapes of the induced CD (ICD) bands obtained for different BBZs. All the spectra were characterized by isoelliptic points that are observed at around 235 and 300 nm for the BBZ: oligo complexes. An upbeat ICD band was observed at 347 to 351 nm on continuous addition of **11a**, **12a**, **12b**, and Hoechst 33342 to oligos, with intensity kept augmenting with increasing BBZ/oligo ratios. With oligo-1, upon addition of BBZ, we observed saturation in the ellipticity value at $r = 2$ that suggests binding of ligands to DNA was 1:1 per binding site. We observed a shoulder at around 272−290 nm in the CD spectra of complexes of **11a**, **12a**, and **12b** with oligo-1, which is similar to Hoechst 33342. These positive ICD signals indicate a minor groove-binding mode of these ligands. The interaction of the BBZ does not alter the conserved CD spectrum of the oligo-1. In the case of oligo-2, all the BBZs, including Hoechst 33342, gave ICD signals on the interaction with oligo-2 in the 348−352 nm region (Figure 5). In general, the strength of the induced band due to complex formation between BBZ and oligo-2 is weak compared with oligo-1 complexes. With oligo-2, the intensity of CD signals increased with increasing the *r*-value and saturation observed at a higher ratio of 4−4.5 (Figure S77). Thus, the constant increase in the CD signal upon increasing the ligand concentration suggests non-specific interactions with oligo 2.

Overall, we established that the newly synthesized ligands have strong and stable binding with AT-rich oligo-1: d-$(CGCGAATTCGCG)_2$ than GC mix oligo-2, and the BBZ/oligo-1 complex is stabilized by hydrogen bonds between the two N−H hydrogen-bond donors in the imidazole rings and adenine N3 and thymine O2 acceptors in the minor groove of the oligonucleotide. A general preference for AT regions is conferred by electrostatic potential and by narrowing the walls of the groove. We hypothesize that local point-by-point AT specificity follows from close van der Waals contacts between ring hydrogen atoms in BBZ and the C2 hydrogens of adenines. It was reported in the literature that replacement of one benzimidazole ring by purine can make that particular molecule GC tolerant, which was also observed by the substitution of the imidazole ring in place of pyrrole in lexitropsins. This supports our observation that BBZs preferentially bind to AT-rich DNA.

Cell Viability Assay of BBZs on the Panel of 60 Cancer Cell Lines. The preliminary screening by cytotoxicity assay on

https://doi.org/10.1021/acsomega.1c05743
ACS Omega 2022, 7, 2861−2880

cancerous cell lines was performed to identify the anticancer potential of BBZs.[71−73] Only 13 BBZs, out of 16 were submitted to the NCI, USA, for evaluation of their single-dose (10 μM) in vitro anticancer activity against complete NCI60 cell lines (Supporting File II), representing mammalian leukemia, melanoma, lung, colon, brain, breast, ovary, kidney, and prostate cancer cell line panels. The selected compounds were further tested for five dose screening (0.01, 0.1, 1, 10 and 100 μM) (Supporting File III). The HCl salt of **13a**, **13d**, and **13c** was precipitating in cell culture media; hence, these were not used for screening (Table 4).

The **12b** showed the highest toxicity against K562 hematopoietic malignant cells and human lymphoma cells (SR) among leukemia cells. While in melanoma cell line panel LOX IMVI, human epithelial melanoma cells, MALME-3M, metastatic malignant melanoma, and M14, human melanoma cells were more sensitive to **11a**, **12a**, and **12b** out of 13 molecules. On the other hand, lesser activity of **11a** and **12a** was found against non-small cell lung, renal, and ovarian carcinoma cells with mean $GI_{50} \geq 5$ μM. These molecules were ineffective against NCI/ADR-RES of the ovarian cancer cell line panel. The mean GI_{50} value suggests the potent anticancer activity of **12b** against leukemia and colon carcinoma cell lines. However, **12b** has been found to be highly sensitive to a few of the most frequently diagnosed cancer types worldwide, such as lung cancer (A549 and NCI460), breast cancer (MCF-7), and prostate cancer (PC-3 and DU-145). The LC_{50} value indicates the toxicity profile of the molecules, that is, the higher the LC_{50}, the lower the toxicity. Noticeably, **11a** was found to be the least toxic for all the cell lines of the leukemia panel ($LC_{50} > 100$). However, both the molecules, **11a** and **12b** are toxic in renal cancer, CNS cancer, and prostate cancer cell line panels ($LC_{50} < 10$). Interestingly, all the three screened BBZs, that is, **11a**, **12a**, and **12b** have shown toxicity in melanoma cell line panels ($LC_{50} < 10$). The cytotoxicity study was also performed in normal transformed cell lines (HEK and NIH3T3) using 3-(4,5-dimethylthiazole-2-yl)2,5-diphenyltetrazolium (MTT), and 50% inhibitory concentration (IC_{50}) was calculated, as shown in Table 5. The molecules were found to be less toxic to normal cells as compared to cancerous cell lines.

Table 5. Cytotoxicity Study on the Normal Cell Line by MTT Assay

		IC_{50} (μM) 48 h	
s. no.	compounds	HEK	NIH3T3
1	**11a**	14.4	2.3
2	**12a**	2.7	8.2
3	**12b**	2.7	3.2

Inhibition of DNA Relaxation Activity HuTopoI Enzyme by BBZ Derivatives. Furthermore, these molecules were screened against Hu Topo I to check whether they have any effect on HuTopoI activity as parent analogues Hoechst 33342 and 33258 are known as HuTopoI inhibitors. DNA relaxation inhibition assays[74,75] were performed on 13 molecules, but only three compounds, **11a**, **12a**, and **12b**, showed inhibition of Hu Topo I (Figure 6a−c). We have included the results of only those three here. The compound **12b** showed 50% inhibition of topoI activity at 16 μm, but the other two compounds, **11a** and **12a**, did show IC_{90} at 140 and 152 μM concentration (Figure 6d). On the other hand, CPT showed 85% inhibition at 25 μM concentration.

Effect of BBZ Derivatives on Cell Cycle Progression in MDA-MB-231 Cells. The triple-negative breast cancers are highly aggressive, with low survival rates and recurrence in patients worldwide. The treatment of triple-negative cancer is still a challenge.[76] To further evaluate the BBZ-mediated inhibition of cell proliferation and its correlation with cell cycle progression, MDA-MB-231 was treated with **11a**, **12a**, and **12b** at their respective GI_{50} concentration (Table 4). After the treatment of cells with the molecules, the cell cycle distribution at different time points was assessed by flow cytometry after propidium iodide (PI) staining (Figure 7a). A significant G2/M arrest was observed through cell cycle analysis with **11a** and **12b** (Figure 7b,c). These results indicate that **11a** and **12b** treated cells increase the G2/M cell population from 2 h onward.

The **12b** treated MDA-MB-231 cells showed an enhanced sub-G1 region, that is, apoptotic cells. At 6 and 12 h, 7.4% of cells was observed in the sub-G1 phase, which is much higher than control cells (1−2%). Thus, an increase in the sub-G1 and G2/M phase reflects the irreparable double-strand DNA damage, causing apoptotic cell death. Our most potent molecule emerged to be **12a**, causing maximum apoptotic cell death.

CONCLUSIONS

The results obtained from this work identify various areas of valuable information relating to ligand-DNA interactions which could be useful for rational drug design and helpful in the development of their potential pharmaceutical and biological effect. In our study, by substituting BBZ with different groups, we synthesized compounds with strong binding affinity with AT sequence of DNA and potent anticancer activity. The docking study of these compounds showed considerable binding affinity and probable interactions with the binary complex of the DNA + Hu Topo I enzyme. The binding affinity was observed to be the highest for three molecules, **11a**, **12a**, and **12b**. Electrophoretic methods showed that the **11a**, **12a**, and **12b** compounds influence the activity of Hu TopoI as a minor groove binder. Topoisomerase inhibitors inhibit DNA synthesis, which can lead to the arrest of the cell cycle in the G2 phase. However, only **11a** and **12b** showed a prominent G2/M arrest of the cell cycle, leading to the cell death. Interestingly, we found that **11a** and **12a** having electron-donating groups at the phenyl ring, viz, 3,4-diethoxy and increased carbon chain length at the piperazine ring showed better cytotoxicity to cancerous cells. However, **12b** with the electron-withdrawing group, CF_3, at the phenyl ring showed strong cytotoxicity against cancerous cell lines. The other synthesized BBZ molecules with tri-methoxy and 2,5-dimethoxy substitution at the phenyl end and *N*,*N*-dimethyl aminoethyl alkyl chain at the piperazine end demonstrated less binding affinity due to the steric hindrance. This suggests that longer propyl and butyl carbon chains at the piperazine end are responsible for increased binding affinity and efficacy. Also, it was evident by our spectroscopic studies that BBZ molecules bind in a non-cooperative manner to DNA while increasing the ligand-DNA ratio to 2. Thus, experimental studies proved that a combination of the $-CF_3$ group at the phenyl ring and the longer alkyl chain at the piperazine ring is one of the probable combinations leading to toxicity to cancer cells, and therefore, it can be exploited further for the development of new selective small molecules as a drug candidate.

https://doi.org/10.1021/acsomega.1c05743
ACS Omega 2022, 7, 2861−2880

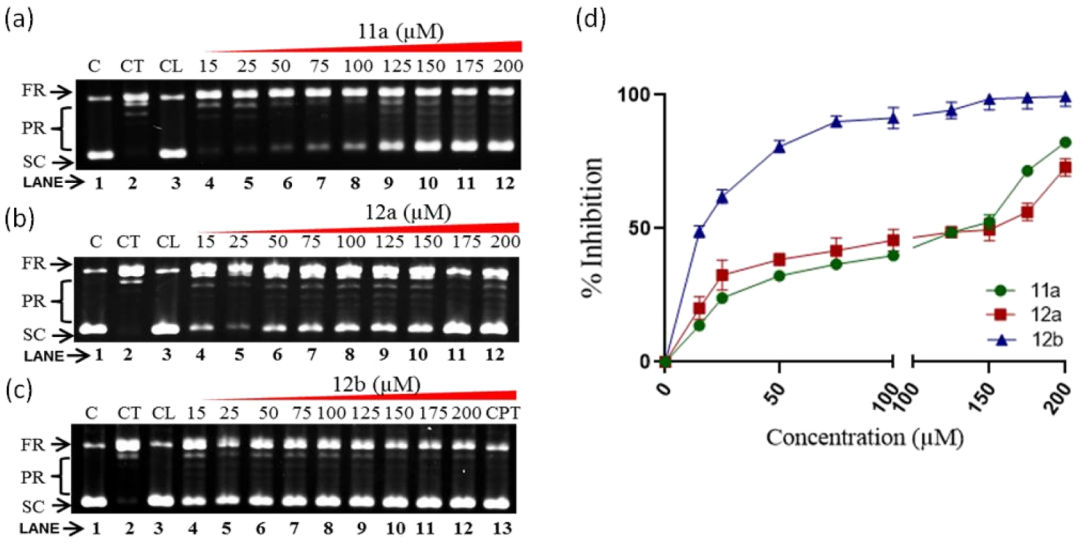

Figure 6. Plasmid DNA relaxation mediated by Hu TopoI in the presence of an increasing concentration of compound CPT, **11a**, **12a**, and **12b** by Hu Topo I.FR (fully relaxed); PR (partially relaxed); and SC (supercoiled). (a–c) Ethidium bromide-stained agarose gel showing: lane 1, pHOT1 plasmid DNA (C); lane 2, relaxation of plasmid DNA by HuTopoI (CT); lane 3, plasmid DNA in the presence of compound (CL); and lanes 4–12, inhibition of relaxation of plasmid DNA by HuTopoI in the presence of 15, 25, 50, 75, 100, 125, 150, 175, and 200 μM of compounds, respectively. The CPT was used at a fixed concentration of 25 μM in this experiment (d); densitometry of relaxation gel was carried out, values were normalized against enzyme control and control, and the final values were plotted in Graph Pad Prism 9. The 50% inhibitory concentrations (IC_{50}) of compounds were calculated by Origin 2019. All experiments were carried out in both biological and technical triplicates.

MATERIALS AND METHODS

All melting points were determined using BUCHI B540 appliances. The ^{1}H (400/500 MHz) and ^{13}C NMR (400 MHz) spectra were observed with the solvents $CDCl_3$ and DMSO-d_6 on an ECX-400P. Jeol chemical shifts are identified in ppm by assigning $CDCl_3$ and DMSO-d_6 with resonance as 7.26 and 2.49 ppm in the ^{1}H NMR spectrum and 77.23 and 39.50 ppm in the ^{13}C NMR spectrum. The coupling constant (J) in hertz (Hz) is reported. On the Agilent 6520 Accurate Mass Q-TOF LC/MS mass spectrometer, HRMS spectra were measured, and IR spectra were taken on a PerkinElmer, FT-IR system. The development of all reactions was recorded by thin-layer chromatography (TLC), which was completed with silica gel 60 (F-254, Merck) pre-coated aluminum sheets with a thickness of 0.25 mm on 20 cm. The TLC plates developed were seen under ultraviolet light (254–366 nm) and treated with iodine vapor. For the purification of intermediate and final compounds, chromatography of the silica gel column was performed. The purity of compounds was found to be greater than 90%. Commercially available reagents were used without further purification unless otherwise stated. The anhydrous organic solvents (e.g., ether, ethyl acetate, chloroform, methanol, ethanol, ACN, DMF, hexane, toluene, etc.) were purchased from commercial sources and used as stated. Chemical reagents, synthesized oligos, d-$(CGCGAATTCGCG)_2$, d$(CGATGTACATCG)_2$, QI-Aquick nucleotide removal kit (Qiagen catalogue 28304), and Dulbecco's modified Eagle's medium (DMEM) were purchased from Sigma. The MDA-MB-231 and A549 cell lines were procured from National Center for Cell Sciences, Pune, India.

General Procedure for the Synthesis of N-Substituted ((Piperazin-1-yl)-2-nitrophenyl) Acetamide (3a–d). Synthesis of 2-nitroacetanilide derivatives was carried out using the reported procedure.[39] The mixture of *N*-(5-chloro-2-nitrophenyl)acetamide **1** (6.98 mmol) with the respective *N*-substituted piperazine **2a–d** (1.2 equiv, 8.37 mmol) and TEA (3.0 equiv, 20.94 mmol) in 10 mL of DMSO was taken in a 250 mL round-bottom flask. The resulting reaction mixture was stirred at 120 °C for 6 h. The reaction was followed by TLC till the completion of the reaction; the reaction mixture was poured on ice-cold water, resulting in a solid precipitate, followed by filtration and drying overnight will give the crude product mixture. Then, the crude mixture was purified by column chromatography over silica gel (60–120 mesh size) using 10–15% MeOH in DCM as the mobile phase, and the product was obtained as a yellow solid with a quantitative yield 72–98% of the (piperazin-1-yl)-2-nitrophenyl) acetamide compounds. The spectra of **3a**, **3b**, and **3d** are not included in the Supporting Information because these compounds are synthesized using the reported procedure.[59]

*N-(5-(4-Methylpiperazin-1-yl)-2-nitrophenyl)acetamide (**3a**).* This compound was synthesized using the reported procedure:[39] yellow solid (92.7% yield, 1.8 g); mp 152.5–153 °C. HRMS (ESI) m/z: calcd for $C_{13}H_{18}N_4O_3$ $[M + H]^+$, 279.1478; obsd, 279.1475.

*N-(5-(4-Allylpiperazin-1-yl)-2-nitrophenyl)acetamide (**3b**).* This compound was synthesized using the reported procedure:[59] yellow solid (93% yield, 2.1 g); mp 143.5–144.5 °C. HRMS (ESI) m/z: calcd for $C_{15}H_{22}N_4O_3$ $[M + H]^+$, 305.1567; obsd, 305.1563.

*N-(5-(4-Butylpiperazin-1-yl)-2-nitrophenyl)acetamide (**3c**).* The product was obtained as a yellow solid (73.8% yield, 1.65 g); mp 95.6–98.4 °C. ^{1}H NMR (400 MHz, DMSO-d_6): δ ppm 0.85–0.89 (t, J = 7.64 Hz, 3H), 1.31–1.27 (m, 2H), 1.41–1.34 (m, 2H), 2.13 (s, 3H), 2.28–2.26 (m, 2H), 2.49–2.43 (m, 4H), 3.39–3.32 (m, 4H), 6.19 (s, 1H), 6.67 (dd, J = 9.9, 3.0 Hz, 1H), 7.67 (d, 1H), 7.96 (d, J = 9.9, 1H), 10.4 (s 1H). ^{13}C NMR (100 MHz, DMSO-d_6): δ ppm 14.0, 20.6, 25.2, 28.8, 46.7, 52.7, 57.8, 104.8, 109.2, 128.2, 128.4, 136.6, 155.1, 169.5. HRMS (ESI) m/z: calcd for $C_{16}H_{24}N_4O_3$ $[M + H]^+$, 321.1878; obsd, 321.1875.

https://doi.org/10.1021/acsomega.1c05743
ACS Omega 2022, 7, 2861–2880

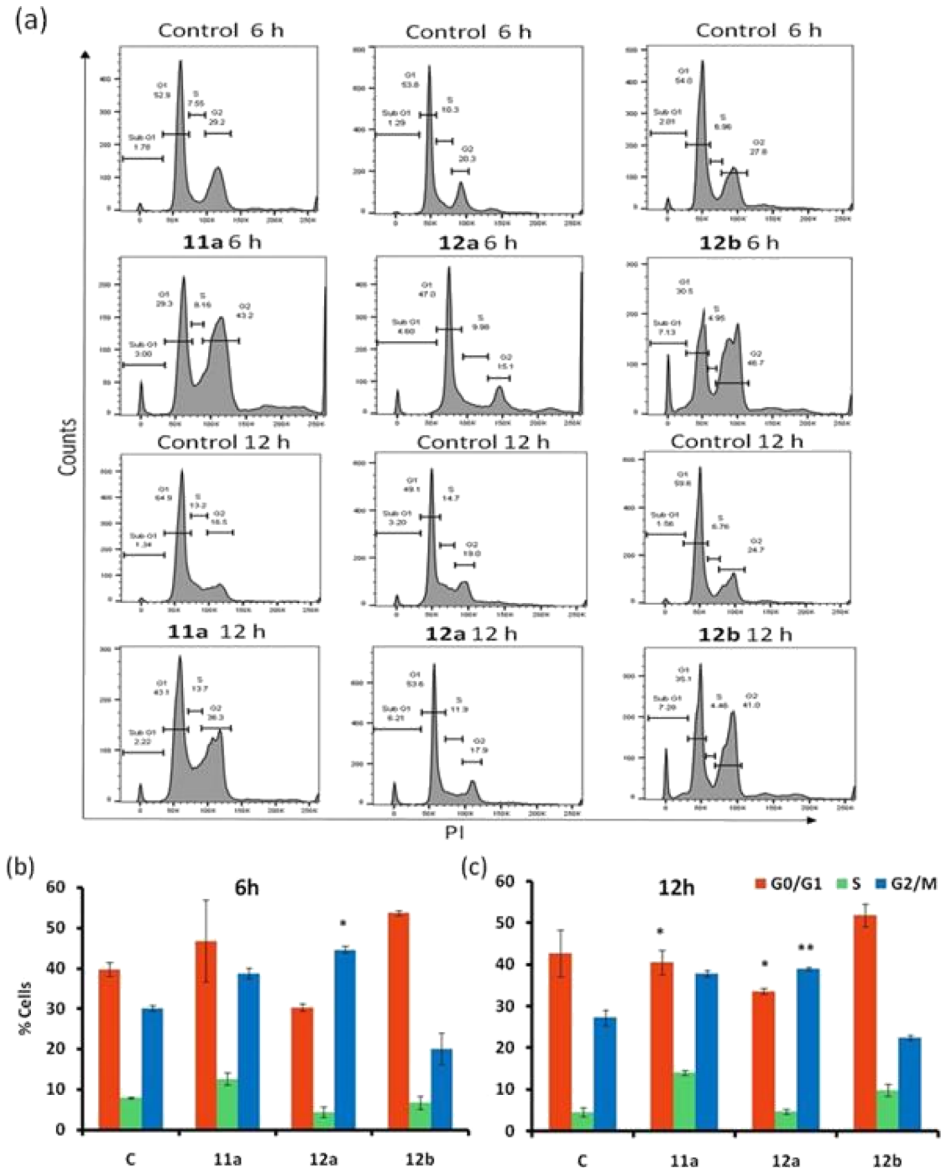

Figure 7. (a) Representative cell cycle analysis at 6 and 12 h post-treatment with three molecules. (b) After treatment with **11a** and **12b**, the % of cells at 6 h in the G2/M phase rises to 38.8 and 44%, respectively, from 27% in untreated cells (average values of three biological repeats). (c) Marked increase in the G2/M phase was prominently maintained till 12 h with 37.8 and 39% in **11a** and **12b**, respectively. **11a** and **12b** showed marked G2/M arrest and increase in sub-G1 population as compared to control at 6 and 12 h, respectively. Data shown are expressed as ±SD repeated in triplicates for each ligand; $*p < 0.05$ and $**p < 0.01$, respectively. There were no significant changes observed in the cell cycle distribution of **12a** treated cells as compared to untreated cells.

*5-[4-(2-(N,N-Dimethyaminoethyl))-1-piperazinyl]-2 Nitroacetanilide (**3d**).* This compound was synthesized using the reported procedure:[59] yellow solid (81.2% yield, 1.9 g); mp 166.2−168.7 °C. HRMS (ESI) *m*/*z*: calcd for $C_{16}H_{25}N_5O_3$ $[M + H]^+$, 336.2035; obsd, 336.2032.

General Procedure for the Synthesis of N-Substituted (Piperazin-1-yl)-2-nitroaniline (4a−d). Synthesis of 2-nitroaniline derivatives was carried out using the reported procedure.[59] Deacetylation of the compound **3a−d** (3.59 mmol 1 equiv) was carried out with 10% H_2SO_4 in a round-bottom flask, and H_2SO_4 solution was added to it (10 mL/g). The resulting reaction mixture was heated at 80 °C till the reaction completion. After the reaction completion, the reaction mixture was brought to room temperature and poured onto the crushed ice. This resulted in a yellow-colored solid deacetylated compound. For complete precipitation of the compound, the pH was maintained neutral with 30% ammonia solution. The resulting solid was then filtered, washed with water, and dried to yield the title compound in good yield. The deacetylated products **4a**, **4b**, and **4d** are synthesized using the reported procedure; therefore, the spectra of these compounds are not added in the Supporting Information.[59]

*5-(4-Methylpiperazin-1-yl)-2-nitroaniline (**4a**).* This compound was synthesized using the reported procedure:[38] yellow solid (83.7% yield, 0.710 g); mp 150.2−151.5 °C. HRMS (ESI) *m*/*z*: calcd for $C_{11}H_{16}N_4O_2$ $[M + H]^+$, 236.1367; obsd, 237.1362.

*(4-Allyl-1-piperazinyl)-2-nitroaniline (**4b**).* This compound was synthesized using the reported procedure:[59] yellow solid (94.8% yield, 0.900 g); mp 83.6−85.4 °C. HRMS (ESI) *m*/*z*: calcd for $C_{13}H_{18}N_4O_2$ $[M + H]^+$, 263.1508; obsd, 263.1508.

https://doi.org/10.1021/acsomega.1c05743
ACS Omega 2022, 7, 2861−2880

*5-(4-Butyllpiperazin-1-yl)-2-nitroaniline (**4c**).* The product was obtained as a yellow solid (92% yield, 0.919 g); mp 83.6−85.4 °C. ^{1}H NMR (400 MHz, $CdCl_3$): δ ppm 0.956 (t, J = 6.0 Hz, 3H), 1.39−1.35 (m, 2H), 2.41−2.38 (m, J = 6.4 Hz, 2H), 2.57 (s 4H), 3.39 (s, 4H), 5.96 (s, 1H) 6.16 (s, 2H), 6.30 (d, J = 7.6 Hz, 1H), 8.03 (d, J = 7.6 Hz, 1H). ^{13}C NMR (100 MHz, DMSO-d_6): δ ppm 14.4, 20.6, 28.6, 46.4, 52.7, 58.0, 97.6, 106.1, 123.3, 127.8, 148.8, 155.6. HRMS (ESI) m/z: calcd for $C_{14}H_{22}N_4O_3$ $[M + H]^+$, 279.1816; obsd, 279.1811.

*5-[4-(2-(N,N-Dimethyl amino ethyl))-1-piperazinyl]-2-nitroaniline (**4d**).* This compound was synthesized using the reported procedure:[59] yellow solid (91.2% yield, 0.960 g); mp 142.2−143.8 °C. HRMS (ESI) m/z: calcd for $C_{14}H_{23}N_5O_2$ $[M + H]^+$, 294.1930; obsd, 294.2047.

General Procedure for the Synthesis of *N*-4-(4-Substituted piperazinyl)-1-phenylenediamine (5a−d). Compounds **4a−d** dissolved in 100 mL, with a ratio of EtOAc/MeOH (4:1), was hydrogenated at room temperature under 40 psi H_2 pressure with a catalytic amount of 10% Pd/C until TLC showed the disappearance of starting material, and the reaction mixture becomes colorless. The reaction mixture was filtered through a Celite bed, and the filtrate was used for the next step without further purification and delay.

General Procedure for Preparation of 2-Aryl-5-cyanobenzimidazoles (8a−e). Synthesis of 2-aryl-5-cyano-benzimidazoles derivatives was carried out using the reported procedure.[59] To freshly prepared ethanolic solution of 4-cyano-1,2-phenylenediamine 6 (3.75 mmol, 1.0 equiv), reacting with the mixture of respective aldehyde **7a−e** (1.5 equiv, 5.6 mmol) and solution of $Na_2S_2O_5$ (0.5 equiv, 1.9 mmol) in water 2.5 mL (1 mL/150 mg) were added. The resulting solution was stirred at reflux for 5−6 h, then cooled to room temperature, and filtered through a Celite bed. The solvents were evaporated under reduced pressure. The crude residue was purified by chromatography on silica gel (60−120 mesh size) in EtOAc/hexane as a solvent mixture to achieve a solid in 64−78% isolated yield. The spectra of **8e** are not included in the Supporting Information because these compounds are synthesized using the reported procedure.[59]

*2-(3,4-Diethoxyphenyl)-1H-benzo[d]imidazole-6-carbonitrile (**8a**).* This compound was purified by column chromatography using a gradient of 35% of EtOAc in hexane, and the product was obtained as an off-white solid (71.5% yield, 0.826 g); mp 198 °C. ^{1}H NMR (400 MHz, DMSO-d_6): δ ppm 1.3−1.4 (m, 6H), 4.03 (m, 4H), 7.11 (dd, J = 18.32, 8.4 Hz, 1H), 7.55 (d, J = 7.64 Hz, 1H), 7.68 (d, J = 9.92 Hz, 1H). 7.72 (s, 1H), 7.76 (s, 1H), 8.13 (s, 1H), 13.2 (s, 1H). ^{13}C NMR (100 MHz, DMSO-d_6); 14.7, 63.9, 96.8, 103.6, 111.2, 112.9, 113.2, 115.6, 120.0, 121.4, 122.4, 125.5, 134.6, 140.2, 148.2, 150.3. HRMS (ESI) m/z: calcd for $C_{18}H_{17}N_3O_2$ $[M + H]^+$, 308.1399; obsd, 308.1387.

*2-(4-(Trifluoromethyl)phenyl)-1H-benzo[d]imidazole-6-carbonitrile (**8b**).* This compound was purified by column chromatography using a gradient of 30% of EtOAc in hexane, and the product was obtained as an off-white solid (69.5% yield, 0.750 g); mp 215−217 °C. ^{1}H NMR (400 MHz, DMSO-d_6): δ ppm 7.61 (d, J = 7.64 Hz, 1H), 7.77 (d, J = 7.64 Hz 1H), 7.93 (d, J = 8.4 Hz, 2H), 8.10 (s, 1H), 8.30 (d, J = 8.4 Hz, 2H). ^{13}C NMR (100 MHz, DMSO-d_6): δ ppm 104.5, 119.8, 12.6, 125.3, 126.0 (q, J = 3.86 Hz, 1C), 126.76 (d J = 3.86 Hz, 1C), 128.0, 129.8, 130.2, 130.4, 130.8, 132.9, 152.8. HRMS (ESI) m/z: calcd for $C_{15}H_8N_3F_3$ $[M + H]^+$, 288.0739; obsd, 288.0745.

*2-(2,5-Dimethoxyphenyl)-1H-benzo[d]imidazole-5-carbonitrile (**8c**).* This compound was purified by column chromatography using a gradient of 35% of EtOAC in hexane, and the product was obtained as an off-white solid (66.7% yield, 0.700 g); mp 235−237 °C. ^{1}H NMR (400 MHz, DMSO-d_6): δ ppm 3.81 (s, 1H), 3.83 (s, 1H), 7.10 (d, J = 8.4 Hz, 1H), 7.52 (d, J = 8.0 Hz, 1H), 7.74 (s, 2H), 7.67 (s, 1H), 8.07 (s, 1H), 13.26 (s, 1H). ^{13}C NMR (100 MHz, DMSO-d_6): δ ppm 56.13, 104.13, 110.42, 112.30, 120.50, 120.69, 122.10, 125.98, 149.45, 151.48. HRMS (ESI) m/z: calcd for C_{16} $H_{14}N_2O_2$ $[M + H]^+$, 280.1086; obsd, 280.1060.

*2-(3,4,5-Trimethoxyphenyl)-1H-benzo[d]imidazole-6-carbonitrile (**8d**).* This compound was synthesized using the reported procedure[39] and purified by column chromatography using a gradient of 35% of EtOAc in hexane, and the product was eluted as an off-white solid (64.5% yield, 0.750 g); mp 240−238 °C. ^{1}H NMR (400 MHz, DMSO-d_6): δ ppm 3.73 (s, 3H), 3.89 (s, 6H), 7.54 (d, J = 11.44 Hz, 2H), 7.58 (d, J = 10.68 Hz, 1H), 7.70 (d, J = 9.16 Hz, 1H), 8.12 (d, J = 9.16 Hz, 1H), 13.3 (s, 1H). ^{13}C NMR (100 MHz, DMSO-d_6): δ ppm 56.11, 60.2, 104.2, 112.6, 116.3, 119.7, 119.9, 123.3, 124.3, 125.3, 125.9, 138.1, 139.5, 143.2, 153.3, 154.0, 154.8. HRMS (ESI) m/z: calcd for $C_{17}H_{16}N_2O_4$ $[M + H]^+$, 310.1180; obsd, 310.1187.

*2-(4-Ethoxyphenyl)-1H-benzo[d]imidazole-6-carbonitrile (**8e**).* This compound was synthesized using the known procedure[59] and purified by silica gel column chromatography using a gradient of 25% of EtOAc in hexane, and the product was eluted as a white solid (72.8% yield, 0.720 g); mp 223.1−224.8 °C. HRMS (ESI) m/z: calcd for $C_{16}H_{13}N_3O$ $[M + H]^+$, 264.1137; obsd, 264.1129.

General Procedure for the Preparation of 2-Aryl-5-formylbenzimidazoles (9a−e). Ni−Al alloy (1.2 equiv, 0.036 mmol) was added to a solution of **8a−8f** (2.6 mmol 1 equiv) in 75% aqueous formic acid. The reaction mixture was heated at 95 °C for 3 h under an inert atmosphere. The hot mixture was filtered through a Celite bed, and the reaction flask was rinsed with water (2 × 10 mL). The aqueous solution was concentrated to dryness. After the addition of water to this residue, a precipitate was formed. The pH of this suspension was adjusted to 9.0 by the dropwise addition of 2 N NaOH, and the product was then extracted into ethyl acetate. The organic layers were dried over anhydrous Na_2SO_4 and filtered. The solvents were evaporated under reduced pressure. The residue was purified by chromatography on silica gel (60−120 mesh size) using the gradient MeOH/EtOAc in the range of 3:97 to 6:94 to obtain the product as a solid in 67−93% yield. The spectra of **9e**, **9f** are not added in the Supporting Information because these compounds are synthesized using the reported procedure.[59]

*2-(3,4-Diethoxyphenyl)-1H-benzo[d]imidazole-6-carbaldehyde (**9a**).* The product was obtained as an off-white solid (80% yield, 0.650 g); mp 110 °C. ^{1}H NMR (400 MHz, DMSO-d_6): δ ppm 1.40−1.30 (m, 6H), 4.13−4.02 (m, 4H), 5.73 (br, s, 1H), 7.08 (d, J = 9.16, 1H), 7.69 (d, J = 8.4 Hz, 1H), 7.73 (d, J = 8.4 Hz, 1H), 7.70 (s, 1H), 8.10 (s, 1H), 8.20 (d, J = 8.4 Hz, 1H), 10.01 (s, 1H). ^{13}C NMR (100 MHz, DMSO-d_6): δ ppm 14.7, 63.9, 111.2, 112.9, 115.1, 117.8, 120.0, 121.7, 122.4, 122.9, 131.0, 148.2, 150.3, 154.7, 163.6, 192.5. HRMS (ESI) m/z: calcd for $C_{18}H_{19}N_2O_3$ $[M + H]^+$, 311.1396; obsd, 311.1398.

*2-(4-(Trifluoromethyl)phenyl)-1H-benzo[d]imidazole-6-carbaldehyde (**9b**).* The product was obtained as an off-white solid (93.5% yield, 0.713 g); mp 160 °C. ^{1}H NMR (400 MHz, DMSO-d_6): δ ppm 5.80 (s, 1H), 7.87 (d, J = 8.4 Hz, 1H), 7.92 (d, J = 8.4 Hz, 2H), 8.11 (d, J = 18.2 Hz, 1H), 8.25 (s, 1H), 8.37 (d, J = 16.8 Hz, 2H), 10.04 (s, 1H). ^{13}C NMR (100 MHz, DMSO-d_6): δ ppm 112.4, 120.1, 122.6, 125.39, 126.05 (q, J =

https://doi.org/10.1021/acsomega.1c05743
ACS Omega 2022, 7, 2861−2880

3.83 Hz), 125.86 (d, J = 3.83 Hz, 1C), 126.9, 127.4, 128.18, 130.0, 131.5, 133.2, 152.2, 192.5. HRMS (ESI) m/z: calcd $C_{15}H_{10}N_2F_3O$ $[M + H]^+$, 291.0745; obsd, 291.0748.

*2-(2,5-Dimethoxyphenyl)-1H-benzo[d]imidazole-5-carbaldehyde (**9c**).* The product was obtained as an off-white solid (91.7% yield, 0.680 g); mp 230−232 °C. ^{1}H NMR (400 MHz, $CDCl_3$): δ ppm 3.81 (s, 3H), 3.92 (s, 3H), 6.92 (d, J = 6.4 Hz, 1H), 7.67 (d, J = 6.8 Hz, 2H), 7.75 (s, 1H), 7.8 (d, J = 6.8 Hz, 1H), 8.10 (s, 1H), 10.04 (s 1H). ^{13}C NMR (100 MHz, DMSO-d_6): δ ppm 56.10, 110.31, 112.31, 114.20, 119.27, 120.28, 122.37, 123.53, 131.56, 135.53, 140.25, 144.24, 149.45, 151.29, 154.51, 193.1. HRMS (ESI) m/z: calcd $C_{16}H_{15}N_2O_3$ $[M + H]^+$, 283.1083; obsd, 283.1060.

*2-(3,4,5-Trimethoxyphenyl)-1H-benzo[d]imidazole-6-carbaldehyde (**9d**).* The compound was synthesized using the reported procedure:[39] off-white solid (84% yield, 0.690 g); mp 198 °C. ^{1}H NMR (400 MHz, DMSO-d_6): δ ppm 3.69 (s, 3H), 3.84 (s, 6H), 7.54 (s, 2H), 7.75 (s, 2H), 8.13 (s 1H), 10.03 (s, 1H). ^{13}C NMR (100 MHz, DMSO-d_6): δ ppm 56.09, 60.2, 104.2, 123.0, 124.6, 131.2, 139.3, 153.3, 163.6, 192.5. HRMS (ESI) m/z: calcd for $C_{17}H_{17}N_2O_4$ $[M + H]^+$, 313.119; obsd, 313.1190.

*2-(4-Ethoxyphenyl)-1H-benzo[d]imidazole-6-carbaldehyde (**9e**).* This compound was synthesized using the reported procedure:[59] off-white solid (70.8% yield, 0.499 g); mp 266.8−268.6 °C. HRMS (ESI) m/z: calcd for $C_{16}H_{14}N_2O_2$ $[M + H]^+$, 267.1133; obsd, 267.1125.

General Procedure for Preparation of BBZs (10a−c, 11a−d, and 12a−e). To the freshly prepared ethanolic solution of *N*-4-(4-substituted piperazinyl)-1phenylenediamine (1.46 mmol, 1 equiv) **5a−d**, a mixture of respective aldehyde **9a−e** (2.2 mmol, 1.5 equiv) and solution of $Na_2S_2O_5$ (0.73 mmol, 0.5 equiv) in water (1 mL/150 mg) were added in 20 mL of ethanol. The resulting solution was stirred at reflux for 24 h, then cooled to room temperature, and filtered through a bed of Celite. The solvents were evaporated under reduced pressure. The crude residue was purified by chromatography on silica gel (100−200 mesh size) in the MeOH/DCM solvent mixture to afford the solid title compounds in 60−72% yield.

*2-(2-(3,4-Diethoxyphenyl)-1H-benzo[d]imidazol-5-yl)-5-(4-methylpiperazin-1-yl)-1H-benzo[d]imidazole (**10a**).* This compound was purified by column chromatography using a gradient of 12% of MeOH in DCM, and the product was obtained as a light brown crystalline solid (63% yield, 0.450 g); mp 185−186.1 °C. ^{1}H NMR (400 MHz, DMSO-d_6): δ ppm 1.35−1.25 (m, 6H), 2.35 (s, 3H), 2.70 (s, 4H), 3.14 (s, 4H), 4.12−3.99 (m, 4H), 6.88 (d, J = 7.2 Hz, 1H), 7.00 (s, 1H), 7.05 (d, J = 8.4 Hz, 1H), 7.41 (d, J = 8.8 Hz, 1H), 7.63 (d, J = 8.4 Hz, 1H), 7.78−7.72 (m, 1H), 7.98 (d, J = 8.4 Hz, 1H), 8.20 (s, 1H), 8.29 (s, 1H). ^{13}C NMR (100 MHz, DMSO-d_6): δ ppm 15.1, 43.6, 48.6, 53.6, 64.5, 102.0, 111.6, 113.7, 114.9, 120.1, 121.4, 122.3, 124.6, 135.6, 5, 147.2, 148.6, 150.5, 152.5, 153.9, 167.2. HRMS (ESI) m/z: calcd for $C_{29}H_{32}N_6O_2$ $[M + H]^+$, 497.2610; obsd, 497.2631.

*5-(4-Methylpiperazin-1-yl)-2′-(4-(trifluoromethyl)phenyl)-1H,1′H-2,5′-Bibenzo[d]imidazole (**10b**).* This compound was purified by column chromatography using a gradient of 12% of MeOH in DCM, and the product was obtained as a brown crystalline solid (67.7% yield, 0.470 g); mp 284−285.2 °C. ^{1}H NMR (400 MHz, DMSO-d_6): δ ppm 2.28−2.26 (s, 3H), 2.58−2.52 (s, 4H), 3.15−3.12 (s, 4H), 6.97−6.93 (d, J = 6.8, 2.28 Hz, 1H), 7.04−7.01 (s, 1H), 7.47−7.44 (d, J = 9.16 Hz, 1H), 7.73−7.78 (d, J = 8.4 Hz, 1H), 7.95−7.99 (d, J = 8.4 Hz, 2H), 8.1−8.08 (d, J = 9.16 Hz, 1H), 8.24−8.27 (s, 1H), 8.38 (s, 1H), 8.48−8.44 (d, J = 8.4 Hz, 1H). ^{13}C NMR (100 MHz, DMSO-d_6): δ ppm 45.27, 49.6, 54.6, 113.8, 121.5, 122.8, 125.24, 126.03 (q, J = 3.83 Hz, 4C), 127.0, 127.3, 129.7, 130.0, 133.7, 147.6, 151.1. HRMS (ESI) m/z: calcd for $C_{26}H_{23}F_3N_6$ $[M + H]^+$, 477.2003; obsd, 477.2004.

*2′-(2,5-Dimethoxyphenyl)-6-(4-methylpiperazin-1-yl)-1H,3′H-2,5′-bibenzo[d]imidazole (**10c**).* Purification of this compound by column chromatography using a gradient of 12% of MeOH in DCM, and the product was eluted as a brown solid (70.4% yield, 0.480 g); mp 232−235 °C. ^{1}H NMR (400 MHz, DMSO-d_6): δ ppm 2.40 (s, 3H), 2.75 (s, 4H), 3.18 (s, 4H), 3.78 (s, 3H), 3.96 (s, 3H), 6.90 (d, J = 8.3 Hz, 1H), 7.05−7.01 (m, 2H), 7.16 (d, J = 9.0 Hz, 1H), 7.43 (d, J = 8.5 Hz, 1H), 7.73 (d, J = 8.0 Hz, 1H), 7.86 (s, 1H), 8.01 (s, 1H), 8.40 (s, 1H), 12.34 (s, 1H). ^{13}C NMR (100 MHz, DMSO-d_6): δ 153.72, 152.30, 151.71, 150.71, 147.62, 125.01, 118.74, 117.92, 114.27, 114.00, 56.71, 56.08, 54.56, 49.59, 44.99. HRMS (ESI) m/z: calcd for $C_{27}H_{29}N_6O_2$ $[M + H]^+$, 469.2352; obsd, 469.2374.

*2-(2-(3,4-Diethoxyphenyl)-1H-benzo[d]imidazol-5-yl)-5-(4-propylpiperazin-1-yl)-1H-benzo[d]imidazole (**11a**).* Purification of this compound by column chromatography using a gradient of 10% of MeOH in DCM, and the product was obtained as a brown crystalline solid (60% yield, 0.460 g); mp 230−231.7 °C. ^{1}H NMR (400 MHz, DMSO-d_6): δ ppm 0.79 (t, J = 6.4 Hz, 3H), 1.34−1.27 (m, 6H), 1.43−1.40 (m, 2H), 2.32 (m, 2H), 2.58 (s, 4H), 3.07 (s, 4H), 4.09−4.01 (m, 4H), 6.84 (d, J = 8.4 Hz, 1H), 6.95 (s, 1H), 7.05 (d, J = 8.4 Hz, 1H), 7.37 (d, J = 8.4 Hz, 1H), 7.61 (d, J = 8.4 Hz, 1H), 7.73 (d, J = 5.2 Hz, 2H), 7.95 (d, J = 8.0 Hz, 1H), 8.14 (s, 1H), 8.24 (s, 1H). ^{13}C NMR (100 MHz, DMSO-d_6): δ ppm 11.6, 14.7, 19.03, 49.6, 52.6, 59.7, 111.1, 113.0, 114.0, 119.4, 120.8, 122.3, 124.4, 147.1, 147.1, 150.0, 151.5, 153.3, 163.8. HRMS (ESI) m/z: calcd for $C_{31}H_{36}N_6O_2$ $[M + H]^+$, 525.2963; obsd, 525.2970.

*2-(4-(Trifluoromethyl)phenyl)-5-(5-(4-propylpiperazin-1-yl)-1H-benzo[d]imidazol-2-yl)-1H-benzo[d]imidazole (**11b**).* The compound was purified by column chromatography using a gradient of 10% of MeOH in DCM, and the product was eluted as a light yellow crystalline solid (63.8% yield, 0.470 g); mp 268−270.2 °C. ^{1}H NMR (400 MHz, DMSO-d_6): δ ppm 0.82−0.9 (t, J = 6.84 Hz, 3H), 1.42−1.5 (m, J = 6.84 Hz, 2H), 2.26−2.34 (t, J = 6.8 Hz, 2H), 2.52−2.6 (m, 4H), 3.12−3.06 (m, 4H), 6.92 (d, J = 8.4 Hz, 1H), 7.44 (s, 1H), 7.69 (d, J = 6.12 Hz, 1H), 7.82 (d, J = 6.12 Hz, 1H), 7.95 (d, J = 8.4 Hz, 2H), 8.08 (dd, J = 16.8 Hz, 16.8 Hz, 1H), 8.3 (s, 1H), 8.42 (d, J = 8.4 Hz, 2H), 12.6 (s, 1H), 13.3 (s, 1H). ^{13}C NMR (100 MHz, DMSO-d_6): δ ppm 11.83, 19.4, 49.89, 52.89, 59.7, 109.1, 120.9, 122.8, 125.4, 126.04 (q, J = 3.83 Hz, CF_3), 127.28, 129.33, 129.69, 131.10, 130.31, 133.62, 147.7, 151.1. HRMS (ESI) m/z: calcd for $C_{28}H_{27}F_3N_6$ $[M + H]^+$, 505.2312; obsd, 505.2319.

*2′-(2,5-Dimethoxyphenyl)-6-(4-propylpiperazin-1-yl)-1H,3′H-2,5′-bibenzo[d]imidazole (**11c**).* Purification of this compound by column chromatography using a gradient of 10% of MeOH in DCM, and the product was eluted as a brown solid (71.7% yield, 0.520 g); mp 238−241 °C. ^{1}H NMR (400 MHz, DMSO-d_6): δ ppm 0.91 (t, J = 7.3 Hz, 3H), 1.60 (s, 2H), 2.82 (s, 2H), 3.06 (s, 4H), 3.31 (s, 4H), 3.82 (s, 3H), 4.00 (s, 3H), 6.97 (d, J = 6.6 Hz, 1H), 7.11−7.01 (m, 2H), 7.21 (d, J = 9.1 Hz, 1H), 7.49 (d, J = 7.0 Hz, 1H), 7.77 (d, J = 7.5 Hz, 1H), 7.90 (s, 1H), 8.03 (s, 1H), 8.04 (s, 1H). ^{13}C NMR (100 MHz, DMSO-d_6): δ ppm 164.3, 153.4, 152.1, 151.0, 149.4, 147.8, 124.8, 122.9, 121.2, 120.15, 114.2, 112.2, 110.43, 57.5, 56.17, 53.0, 49.9, 28.2,

https://doi.org/10.1021/acsomega.1c05743
ACS Omega 2022, 7, 2861−2880

20.5, 14.3. HRMS (ESI) m/z: calcd for $C_{29}H_{33}N_6O_2$ $[M + H]^+$, 497.2665; obsd, 497.2684.

*5-(4-Propylpiperazin-1-yl)-2′-(3,4,5-trimethoxyphenyl)-1H,1′H-2,5′-bibenzo[d]imidazole (**11d**).* Purification of this compound by column chromatography using a gradient of 10% of MeOH in DCM, and the product was eluted as a brown crystalline solid (70.2% yield, 0.540 g); mp 250−252.6 °C. ^{1}H NMR (400 MHz, DMSO-d_6): δ ppm 0.82 (t, J = 9.2 Hz, 3H), 1.47−141 (m, 2H), 2.35−2.33 (m, 2H), 2.59 (s, 4H), 3.09 (s, 4H), 3.70 (s, 3H), 3.87 (s, 6H), 6.90−6.84 (dd, J = 9.2, 1H), 6.97 (s, 1H), 7.40 (d, J = 7.2 Hz, 1H), 7.53 (s, 1H), 7.68 (d, J = 8.0 Hz, 1H), 8.00 (d, J = 8.4 Hz, 1H), 8.17 (s, 1H), 8.29 (s 1H). ^{13}C NMR (100 MHz, DMSO-d_6): δ ppm 11.7, 19.0, 49.5, 52.5, 56.1, 59.3, 60.2, 104.1, 114.2, 121.3, 124.4, 125.7, 139.2, 147.1, 151.9, 153.0, 153.3, 164.1. HRMS (ESI) m/z: calcd for $C_{30}H_{34}N_6O_3$ $[M + H]^+$, 527.2749; obsd, 527.2755.

*5-(4-Butylpiperazin-1-yl)-2-(2-(3,4-diethoxyphenyl)-1H-benzo[d]imidazol-5-yl)-1H-benzo[d]imidazole (**12a**).* Purification of this compound by column chromatography using a gradient of 15% of MeOH in DCM, and the product was eluted as a brown crystalline solid (60.2% yield, 0.465 g); mp 255−256.2 °C. ^{1}H NMR (400 MHz, DMSO-d_6): δ ppm 0.82 (d, J = 6.4 Hz, 3H), 1.29−121 (m, 6H), 1.32 (m, 2H), 1.42 (m, 2H), 2.42 (s, 2H), 2.69 (s, 4H) 3.11 (s, 4H), 4.04 (m, 4H), 6.85 (d, J = 8.4 Hz, 1H), 6.96 (s, 1H), 7.04 (d, J = 8.4 Hz, 1H), 7.37 (d, J = 8.0 Hz, 1H), 7.59 (d, J = 8.0 Hz, 1H), 7.74−7.68 (m, 1H), 7.93 (d, J = 8.0 Hz, 1H), 8.10 (s, 1H), 8.23 (s, 1H). ^{13}C NMR (100 MHz, DMSO-d_6): δ ppm 13.8, 14.7, 19.9, 27.6, 49.2, 52.3, 55.1, 56.7, 64.0, 111.0, 112.5, 114.1, 119.3, 120.3, 122.7, 123.9, 146.9, 148.3, 150.4, 152.09, 153.2, 163.5. HRMS (ESI) m/z: calcd for $C_{32}H_{38}N_6O_2$ $[M + H]^+$, 539.3122; obsd, 539.3117.

*5-(5-(4-Butylpiperazin-1-yl)-1H-benzo[d]imidazol-2-yl)2-(4(trifluoromethyl)phenyl)-1H-benzo[d]imidazole (**12b**).* The product was obtained as a light brown crystalline solid (66% yield, 0.500 g); mp 265−266.5 °C. ^{1}H NMR (400 MHz, DMSO-d_6): δ ppm, 0.82−0.78 (t, J = 7.2 Hz, 3H), 1.25−1.15 (m, 2H), 1.39−1.29 (m, J = 2H), 2.28−2.24 (t, J = 7.6 Hz, 2H), 2.49 (m, 4H), 3.047 (m, 4H), 6.86 (dd, J = 8.8, J = 1.6 Hz, 1H), 6.96 (s, 1H), 7.39 (d, J = 8.4, Hz, 1H), 7.71 (d, J = 8.0 Hz, 1H), 7.87 (d, J = 8.8 Hz, 2H), 8.00 (d, J = 8.4 Hz, 1H), 8.29 (d, J = 8.0 Hz, 1H), 8.33 (d, J = 8.0 Hz, 2H). ^{3}C NMR (100 MHz, DMSO-d_6): δ ppm 13.9, 20.1, 28.3, 49.9, 52.9, 57.4, 113.6, 120.0, 122.7, 125.5, 126.0 (q, J = 3.83 Hz, CF_3), 127.7, 128.2, 129.2, 129.7, 130.0, 130.4, 133.6, 147.7, 151.1. HRMS (ESI) m/z: calcd for $C_{29}H_{29}F_3N_6$ $[M + H]^+$, 519.2462; obsd, 519.2467.

*6-(4-Butylpiperazin-1-yl)-2′-(2,5-dimethoxyphenyl)-1H,3′H-2,5′-bibenzo[d]imidazole (**12c**).* Purification of this compound by column chromatography using a gradient of 15% of MeOH in DCM, and the product was obtained as a pale yellow crystalline solid (61.7% yield, 0.460 g); mp 272.5−275 °C. ^{1}H NMR (400 MHz, DMSO-d_6): δ ppm, 0.84−0.80 (t, J = 7.02 Hz, 3H), 1.26−1.18 (m, 2H), 1.42−1.37 (m, 2H), 2.45−2.39 (m, 2H), 2.62 (s, 4H), 3.10 (s, 4H), 3.75 (s, 3H), 3.93 (s, 3H), 6.85 (d, J = 8.6 Hz, 1H), 6.96 (s, 1H), 7.02 (dd, J = 8.8, 2.8 Hz, 1H), 7.13 (d, J = 8.8 Hz, 1H), 7.38 (d, J = 8.4 Hz, 1H), 7.69 (d, J = 8.4 Hz, 1H), 7.84 (d, J = 3.2 Hz, 1H), 8.16 (s, 1H), 8.36 (s, 1H). ^{13}C NMR (100 MHz, DMSO-d_6): δ ppm 164.4, 153.6, 152.2, 151.6, 150.6, 147.8, 124.9, 121.3, 118.7, 117.8, 114.2, 113.9, 57.4, 56.6, 56.0, 52.9, 49.9, 28.1, 20.4, 14.3. HRMS (ESI) m/z: calcd for $C_{30}H_{34}N_6O_2$ $[M + H]^+$, 511.2810; obsd, 511.2815.

*5-(4-Butylpiperazin-1-yl)-2-(2-(3,4,5-trimethoxyphenyl)-1H-benzo[d]imidazol-5-yl)-1H-benzo[d]imidazole (**12d**).* Purification of this compound by column chromatography using a gradient of 15% of MeOH in DCM, and the product was eluted as a brown crystalline solid (64.4% yield, 0.509 g); mp 235−237.1 °C. ^{1}H NMR (400 MHz, DMSO-d_6): δ ppm 0.90−0.87 (t, J = 7.6 Hz, 3H), 1.36−1.27 (m 2H), 1.52−1.42 (m 2H), 2.4−2.39 (t, J = 7.6 Hz, 2H), 2.62 (m, 4H), 3.14 (s, 4H), 3.74 (s, 3H), 3.91 (s, 6H), 6.92 (d, J = 9.16 Hz, 1H), 7.01 (s, 1H), 7.44 (d, J = 8.4 Hz, 1H), 7.56 (s, 2H), 7.71 (d, J = 8.4 Hz, 1H), 8.03 (d, J = 8.4 Hz, 1H), 8.18 (s, 1H), 8.31 (s, 1H). ^{13}C NMR (100 MHz, DMSO-d_6): δ ppm 13.9, 20.0, 28.4, 49.6, 52.7, 56.1, 57.3, 60.2, 104.0, 114.4, 120.7, 125.0, 125.6, 139.3, 147.0, 150.6, 152.4, 153.2, 163.8. HRMS (ESI) m/z: calcd for $C_{31}H_{36}N_6O_3$ $[M + H]^+$, 541.2907; obsd, 541.2917.

*5-(4-Butylpiperazin-1-yl)-2′-(4-ethoxyphenyl)-1H,1′H-2,5′-bibenzo[d]imidazole (**12e**).* Purification of this compound by column chromatography using a gradient of 20% of MeOH in DCM, and the product was obtained as a brown crystalline solid (63.7% yield, 0.460 g); 284−285.2 °C. ^{1}H NMR (400 MHz, DMSO-d_6): δ ppm 0.86 (t, J = 7.6 Hz, 3H), 1.31−1.26 (m, 2H), 1.39−1.31 (m, 3H), 1.46−1.38 (m, 2H), 2.47−2.51 (m, 2H), 2.71 (s, 4H), 3.16 (s, 4H), 4.12−4.06 (m 2H), 6.90 (dd, J = 8.4 Hz, 1H), 7.02 (m, 1H), 7.09 (d, J = 9.16 Hz, 2H), 7.44 (d, J = 9.16 Hz, 1H) 7.65 (d, J = 8.4 Hz, 1H), 8.02 (d, J = 8.4 Hz 1H), 8.15 (d, J = 9.12 Hz, 1H), 8.2 (s, 1H), 8.3 (s, 1H). ^{13}C NMR (100 MHz, DMSO-d_6): δ ppm 13.8, 20.0, 27.6, 49.4, 52.4, 57.2, 63.2, 113.2, 114.3, 120.3, 122.3, 124.3, 128.3, 147.2, 152.1, 153.0, 159.3, 164.0, 172.4. HRMS (ESI) m/z: calcd for $C_{30}H_{34}N_6O_2$ $[M + H]^+$, 495.2856; obsd, 495.2855.

*2-(4-(2′-(3,4-Diethoxyphenyl)-1H,3′H-[2,5′-bibenzo[d]-imidazol]-6-yl)piperazin-1-yl)N,N-dimethylethan-1-amine (**13a**).* Purification of this compound by column chromatography using a gradient of 20% of MeOH in DCM, and the product was eluted as a brown crystalline solid (61.8% yield, 0.500 g); mp 262−2565 °C. ^{1}H NMR (400 MHz, DMSO-d_6): δ ppm 1.37−1.30 (m 6H). 2.43 (s, 6H), 2.55 (m, 2H), 2.56 (s, 4H), 2.77 (m, 2H), 3.09 (s, 4H), 4.14−4.04 (m, 4H), 6.88 (d, J = 8.8 Hz, 1H), 6.98 (s 1H), 7.08 (d, J = 8.8 Hz, 1H), 7.40 (d, J = 8.4 Hz, 1H), 7.63 (d, J = 7.2 Hz, 1H), 7.77 (d, J = 8.4 Hz, 1H), 7.81 (s 1H), 7.99 (d, J = 8.4 Hz, 1H) 8.30 (s, 1H), 13.2 (br, 2H). ^{13}C NMR (100 MHz, DMSO-d_6): δ 153.4, 152.0, 150.9, 149.4, 148.1, 124.9, 122.9, 121.1, 120.1, 114.1, 112.2, 110.4, 109.8, 56.1, 55.4, 54.7, 53.5, 50.4, 44.7. HRMS (ESI) m/z: calcd for $C_{32}H_{39}N_7O_3$ $[M + H]^+$, 553.3238; obsd, 553.3235.

*2-(4-(2′-(4-(Tifluoromethyl)phenyl)-1H,3′H-[2,5′-bibenzo-[d]imidazol]-6-yl)piperazin-1-yl) N,N-Dimethylethan-1-amine (**13b**).* Purification of this compound by column chromatography using a gradient of 18% of MeOH in DCM, and the product was eluted as a light brown crystalline solid (63.5% yield, 0.495 g); mp 250−254 °C. ^{1}H NMR (400 MHz, DMSO-d_6): δ ppm 2 (s, 6H), 2.37 (s, 4H), 2.50 (s, 4H), 3.04 (s, 4H), 6.86 (d, J = 8.8 Hz, 1H), 6.95 (s, 1H), 7.38 (d, J = 8.4 Hz, 1H), 7.71 (d, J = 8.4 Hz, 1H), 7.89 (d, J = 8.4 Hz, 2H), 8.04 (d, J = 8.4 Hz, 1H), 8.35 (s, 1H), 8.40 (d, J = 8.0 Hz, 2H). ^{13}C NMR (100 MHz, DMSO-d_6): δ ppm 151.57, 148.25, 134.21, 130.45, 130.15, 127, 126, 125.97, 123.45, 122.01, 114.20, 60.78, 56.52, 52.72, 53.76, 50.53, 45.80. HRMS (ESI) m/z: calcd for $C_{29}H_{31}F_3N_7$ $[M + H]^+$, 534.2593; obsd, 534.2610.

*2-(4-(2′-(2,5-Dimethoxyphenyl)-1H,3′H-[2,5′-bibenzo[d]-imidazol]-6-yl)piperazin-1-yl)-N,N-dimethylethan-1-amine (**13c**).* Purification of this compound by column chromatography using a gradient of 18% of MeOH in DCM, and the product was obtained as a crystalline solid (61.2% yield, 0.470 g); mp 238−240 °C. ^{1}H NMR (400 MHz, DMSO-d_6): δ ppm

https://doi.org/10.1021/acsomega.1c05743
ACS Omega 2022, 7, 2861−2880

2.36 (s, 6H), 2.47 (m, 2H), 2.55 (m, 4H), 2.67 (m, 2H), 3.07 (s, 4H), 3.81 (s, 3H), 3.87 (s, 3H), 6.88 (d, J = 6.4 Hz, 1H), 6.98 (s, 1H), 7.10 (d, J = 6.0 Hz, 1H), 7.40 (s, 1H), 7.64 (d, J = 6.4 Hz, 2H), 7.83 (s, 2H), 8.00 (d, J = 5.6 Hz, 1H), 8.31 (s, 1H). ^{13}C NMR (100 MHz, DMSO-d_6): δ ppm 153.38, 152.08, 151.04, 149.40, 148.33, 148.13, 124.9, 122.9, 121.1, 120.0, 114.0, 112.2, 110.4, 56.13, 55.48, 54.71, 53.56, 50.49, 44.77. HRMS (ESI) m/z: calcd for $C_{30}H_{34}N_7O_2$ $[M + H]^+$, calcd 526.2916; obsd, 525.2914.

*2-(4-(2′-(3,4,5-Trimethoxyphenyl)-1H,3′H-[2,5′-bibenzo-[d]imidazol]-6-yl)piperazin-1-yl) N,N-Dimethylethan-1-amine (**13d**).* Purification of this compound by column chromatography using a gradient of 18% of MeOH in DCM, and the product was eluted as a light brown crystalline solid (60.9% yield, 0.495 g). ^{1}H NMR (400 MHz, DMSO-d_6): δ ppm 2.50 (m, 6H), 2.56 (m, 4H), 2.88 (m, 2H), 3.03 (s, 2H), 3.06 (s, 4H), 3.66 (s, 3H), 3.83 (s, 6H), 6.85 (d, J = 8.4 Hz, 1H), 7.37 (d, J = 8.4 Hz, 1H), 7.50 (d, J = 16.8 Hz, 1H), 7.57 (s, 1H), 7.62 (s, 2H), 8.00 (d, J = 7.2 Hz, 1H), 8.33 (s, 1H). ^{13}C NMR (100 MHz, DMSO-d_6): δ 153.65, 147.20, 139.56, 124.87, 115.40, 104.43, 60.78, 56.52, 52.72, 48.95, 47.92, 43.31 (d, J = 17.8 Hz). HRMS (ESI) m/z: calcd for $C_{29}H_{31}F_3N_7$ $[M + H]^+$, 556.3018; obsd,. 555.3024.

Molecular Docking Study. The 3D X-crystallographic structure of the crystal structure of Hu Topo I DNA complex (PDB ID: 1EJ9) was retrieved from the RCSB Protein Data Bank (https://www.rcsb.org) and used as a model for molecular docking. The PDB used for this study had 22 bp duplex DNA oligonucleotide along with Hu Topo I protein. We used the glide module[60−62] of the Schrödinger suite for docking of molecules in Hu Topo I: DNA complex. All peptides were prepared using the LigPrep module of the Schrodinger suite and docked in the binding site of protein using the SP-peptide mode of Glide. The receptor grid was generated using the receptor grid generation in the Glide application by specifying the binding (active) site residues, which was identified using the SiteMap tool.[63] The docked conformers were evaluated using Glide (G) Score, and the best-docked pose with the lowest Glide score value was recorded. The most favorable ligand orientation with the lowest free energy (binding affinity) was selected finally for further structural analysis of the protein−ligand complex, which included calculations of hydrogen bonds, hydrophobic interactions, bond lengths, and so on, using Discovery studio visualizer,[64] Maestro of glide module[60−62] of Schrödinger suite, and Ligplot+tools.[65]

UV−Visible Spectroscopy. UV−vis absorbance measurements were performed using a Varian, Cary 300 spectrophotometer instrument with a Peltier temperature control unit. Spectra were acquired using a 1 cm path length cuvette. The 100 μm stock solution of oligo 1 and 2; oligo 1 d-(CGCGAATTCGCG)$_2$ and oligo 2 d(CGATGTACATCG)$_2$, were used for the study. Duplex DNA of d-(GCGCAATTGCGC)$_2$ and d(CGATGTACATCG)$_2$ were made by annealing the complimentary oligonucleotide strands (10 μM each strand) in 20 mM sodium cacodylate buffer containing 100 mM NaCl at pH 7.2. The stock solutions of the ligands (BBZs) of 10 mM concentration were prepared in water and stored at −20 °C. The buffer used for all the studies was 20 mM sodium cacodylate, 100 mM NaCl (pH 7.2). Milli-Q water was used for making buffers. The 1 μm concentration of oligo was titrated 15 times into 5 μM solution of the ligand in cacodylate buffer. DNA binding was marked by hypochromicity or hyperchromicity and red shift of the absorption maxima.[69,70]

UV-Thermal Denaturation. A Cary Varian 300 spectrophotometer equipped with a Peltier thermal programmer was used for the thermal denaturation experiments using stoppered quartz cuvettes of 1 cm optical path length and 1 mL volume. The temperature of the cell holder was increased from 15 to 95 °C and vice versa at a rate of 0.2 °C/min. T_m experiments with oligos 1 and 2 (2.5 μM) in the absence and presence of ligands were carried out at a wavelength of 260 nm as a function of temperature. For T_m experiments, the ligand-oligo ratio, r = 0.5−2 per synthetic oligomers was used. The T_m was determined by plotting the first derivative of the absorbance with respect to temperature (dA_{260}/dT), and T_m is the temperature corresponding to the maximum in the plot. The ΔT_m can be obtained by subtracting the melting temperature of free oligo from that of complex (ligand-oligo).[70] The accuracy of the T_m value is ±1 °C.

Fluorescence Measurement. A Varian, Cary Eclipse instrument was used for equilibrium-binding experiments using a solution of ligand (serially diluted to working concentrations) being excited at its respective λ_{max} (slits of 5 nm), and the resulting emission curves (from 360 to 680 nm) were recorded after serial additions of a concentrated DNA solution (stock 0.1 mM) at 20 °C. After each addition, the solution was mixed by pipetting up and down. The sample equilibrium was monitored by continually exciting and scanning the sample at different times and was usually reached within 3 min. A Scatchard plot of r versus r/c was obtained from the titration data, where r is the ratio of bound ligands (Hoechst 33342, other synthetic analogues) concentration to the total oligo concentrations in base pairs, and c is the concentration of free ligands. The total fluorescence intensity (I_t) was measured by the sum of the contributions from both free and bound ligands as $I_t = I_o(C_t - C_b) + I_bC_b$, where I_o and I_b are fluorescence intensities of the free and fully bound ligand, and C_t and C_b correspond to the total and bound concentrations. From the slope of the plot, the binding constant k is determined for the ligand with oligonucleotides.[69,70]

Circular Dichroism Titrations. CD experiments were carried out at 20 °C using a Jasco J-810 spectropolarimeter. The spectra were recorded at a scan rate of 1 nm/min from 450 to 190 nm wavelength, and an average of three scans was taken. The ICD of the ligands was monitored in the 340−360 nm range. Measurements were carried out in quartz cuvettes of 1 cm optical path length. Duplex DNA of d(GCGCAATTGCGC)$_2$ and d(CGATGTACATCG)$_2$ were made by annealing the complementary oligonucleotide strands (10 μM each strand) in 20 mM sodium cacodylate buffer containing 100 mM NaCl at pH 7.2. The ligand was added to DNA at an increasing ligand/DNA ratio (r = 0.2). Between each ligand addition, an interval of 5 min was maintained, and the samples were mixed by pipetting up and down with a Pasteur pipette.[69,70]

Anticancer Screening Assay. The mammalian cancerous cell lines from the NCI screening panel are grown in RPMI 1640 medium with glutamine, bicarbonate, and 5% fetal calf serum. The cells were inoculated into 96-well plates in 0.2 mL of growth medium at the inoculum densities that depended on the growth characteristics or doubling time of particular cell lines. The compounds to be tested were evaluated at a single dose of 10 μM and then at five different doses prepared by 10-fold dilution starting from as high as 100 μM. The 96-well plates after the addition of respective test compounds were incubated for 48 h at 37 °C in an incubator with 5% CO_2 atmosphere. The cells were fixed in 50 mL of cold 50% (w/v) trichloroacetic acid (TCA), bringing the final concentration of TCA to 10%, and incubated

https://doi.org/10.1021/acsomega.1c05743
ACS Omega 2022, 7, 2861−2880

for 60 min at 4 °C. The supernatant was discarded, and the plate was washed five times with tap water to remove TCA and then air-dried. The staining was carried out by adding 100 mL of sulforhodamine B solution at 0.4% (w/v) in 1% acetic acid being added to each well, and the plates were incubated for 30 min at rt. The unbound dye was removed by washing four times with 1% acetic acid, and the plates were air-dried. The bound dyes were then solubilized in a 10 mM Tris base (pH 10.5), and the absorbance was recorded on an automated plate reader at a wavelength of 564 nm. The percentage growth is calculated using the seven absorbance measurements at time zero (T_0), control growth (C), and five different concentrations of test agents or compounds (TD). Percentage growth inhibition is calculated as $100 \times [(T - T_0)/(C - T_0)]$.[71,72] Three parameters were calculated for each test agent. The 50% growth inhibition (GI_{50}) is the concentration of the test agent, where $100 \times [(T - T_0)/(C - T_0)] = 50$. The ligand concentration resulting in total growth inhibition (TGI) is calculated when: $100 \times [(T - T_0)/(C - T_0)] = 0$. The lethal concentration, LC_{50}, is calculated as where $100 \times [(T - T_0)/T_0] = 50$.

Cytotoxicity Assay. Cytotoxicity was determined using the MTT [3-(4,5-dimethylthiazol-2-yl)-2,5-diphenyl-2*H*-tetrazoliumbromide] assay using a 96-well microtiter plate. 3000 cells per well were plated in 200 μL of the complete medium, and treatment with these ligands was performed 48 h after plating. For IC_{50} determination, cells were exposed continuously with varying concentrations of BBZ, and MTT assays were performed at the end of the fourth day. At the end of the treatment, control and treated cells were incubated with MTT at a final concentration of 0.5 mg/mL for 2 h at 37 °C, and then, the medium was removed. The cells were lysed, and the formazan crystals were dissolved using 150 μL of DMSO. The absorbance was read at 570 nm using 630 nm as the reference wavelength using the TECAN Pro200 reader.[39]

Relaxation Assay of Hu Topo I. Relaxation of negatively supercoiled plasmid DNA by Hu Topo I was assayed in 20 μL of reaction buffer (10 mM Tris−HCl, pH 7.9, 150 mM NaCl, 0.1% BSA, 0.1 mM spermidine, and 5% glycerol) containing 500 ng of supercoiled pHOT1 plasmid DNA and 1 unit of the Hu Topo I enzyme. After incubation at 37 °C for 30 min, the reactions were terminated and analyzed by 1% agarose gel electrophoresis at voltage, as described for Hu Topo I relaxation assay.[74]

Cell Cycle Analysis. Breast cancer cell line MDA-MB 231 was seeded in 35 mm culture plates at a density of 3×10^5 cells/million and cultured for 24 h in DMEM with 1% antibiotic antimycotic solution (Invitrogen) and 10% fetal bovine serum in a 5% humidified CO_2 atmosphere at 37 °C. The cells were then treated with the respective GI_{50} value observed in the MDA-MB-231 cell line of compounds **11a**, **12b**, and **12a**, respectively, for 2 h. The cell was trypsinized, collected, and washed twice with PBS solution at 4 °C. The supernatant was discarded, and the cells were fixed with 70% ethanol. The fixed cells were rinsed with PBS, then stained with the DNA fluorochrome PI (25 μg/mL) and RNase (50 μL of 10 mg/mL), and incubated for 30 min at 37 °C. The samples were then analyzed with a Flow-Activated Cell Sorting equipment (LSR Fortessa, BD Biosciences Pvt. Ltd.) using an FL2 filter (585/40 nm bandpass filter). A minimum of 10,000 events were analyzed for each sample.

Statistical Analysis. Statistical analysis data from three independent experiments are presented as mean ± SD. GI_{50} and LC_{50} values and SD values were calculated by SPSS version 10.0 (SPSS, Inc., Chicago, IL, USA).

■ ASSOCIATED CONTENT

Supporting Information

The Supporting Information is available free of charge at https://pubs.acs.org/doi/10.1021/acsomega.1c05743.

Spectra of ^{1}H NMR, ^{13}C NMR, and HRMS of the synthesized compounds, T_m of the binary complex, UV−visible spectral changes, fluorescence titration spectra, and CD of all BBZ analogues with oligo-1 and oligo-2 (PDF)
Single dose screening of BBZs (PDF)
Five dose screening of selected BBZs against NCI panel of 60 cancer cell lines (PDF)

■ AUTHOR INFORMATION

Corresponding Author

Vibha Tandon − *Special Centre for Molecular Medicine, Jawaharlal Nehru University, New Delhi 110067, India;* orcid.org/0000-0001-6146-937X; Phone: 91-11-26742181; Email: vtandon@mail.jnu.ac.in, vibhadelhi6@gmail.com

Authors

Stuti Pandey − *Department of Chemistry, University of Delhi, Delhi 110007, India; Special Centre for Molecular Medicine, Jawaharlal Nehru University, New Delhi 110067, India*
Pragya Tripathi − *Special Centre for Molecular Medicine, Jawaharlal Nehru University, New Delhi 110067, India*
Palak Parashar − *Special Centre for Molecular Medicine, Jawaharlal Nehru University, New Delhi 110067, India*
Vikas Maurya − *Special Centre for Molecular Medicine, Jawaharlal Nehru University, New Delhi 110067, India*
Md. Zubbair Malik − *Special Centre for Molecular Medicine, Jawaharlal Nehru University, New Delhi 110067, India*
Raja Singh − *Special Centre for Molecular Medicine, Jawaharlal Nehru University, New Delhi 110067, India*
Pooja Yadav − *Special Centre for Molecular Medicine, Jawaharlal Nehru University, New Delhi 110067, India*

Complete contact information is available at: https://pubs.acs.org/10.1021/acsomega.1c05743

Notes

The authors declare no competing financial interest.

■ ACKNOWLEDGMENTS

We are thankful to USIC, the University of Delhi and JNU for the instrumentation facility. S.P. is thankful to DU Non-Net & Council of Scientific and Industrial Research (CSIR) for fellowship. We are grateful to the Department of Biotechnology (DBT) (project no. BT/PR20794/MED/29/1057/2016, dated 27.06.2017), Department of Science and Technology SERB(DST-SERB) (project no. EMR/2017/000454, dated 21.03.2018), DST PURSE (Phase II), UPOE-II Jawaharlal Nehru University, and UGC Mid Term Award grant for funding.

■ REFERENCES

(1) Mann, J.; Baron, A.; Opoku-Boahen, Y.; Johansson, E.; Parkinson, G.; Kelland, L. R.; Neidle, S. A new class of symmetric bisbenzimidazole-based DNA minor groove-binding agents showing antitumor activity. *J. Med. Chem.* **2001**, *44*, 138−144.
(2) Baraldi, P. G.; Bovero, A.; Fruttarolo, F.; Preti, D.; Tabrizi, M. A.; Pavani, M. G.; Romagnoli, R. DNA minor groove binders as potential antitumor and antimicrobial agents. *Med. Res. Rev.* **2004**, *24*, 475−528.
(3) Matsuba, Y.; Edatsugi, H.; Mita, I.; Matsunaga, A.; Nakanishi, O. A novel synthetic DNA minor groove binder, MS-247: Antitumor activity

and cytotoxic mechanism. *Cancer Chemother. Pharmacol.* **2000**, *46*, 1−9.
(4) Khalaf, A. I.; Bourdin, C.; Breen, D.; Donoghue, G.; Scott, F. J.; Suckling, C. J.; Macmillan, D.; Clements, C.; Fox, K.; Sekibo, D. A. T. Design, synthesis and antibacterial activity of minor groove binders: The role of non-cationic tail groups. *Eur. J. Med. Chem.* **2012**, *56*, 39−47.
(5) Bhaduri, S.; Ranjan, N.; Arya, D. P. An overview of recent advances in duplex DNA recognition by small molecules. *Beilstein J. Org. Chem.* **2018**, *14*, 1051−1086.
(6) Wang, L.; Bailly, C.; Kumar, A.; Ding, D.; Bajic, M.; Boykin, D. W.; Wilson, W. D. Specific molecular recognition of mixed nucleic acid sequences: An aromatic dication that binds in the DNA minor groove as a dimer. *Proc. Natl. Acad. Sci. U.S.A.* **2000**, *97*, 12−16.
(7) Cai, X.; Gray, P. J.; Von Hoff, D. D. DNA minor groove binders: Back in the groove. *Cancer Treat. Rev.* **2009**, *35*, 437−450.
(8) Palchaudhuri, R.; Hergenrother, P. J. DNA as a target for anticancer compounds: methods to determine the mode of binding and the mechanism of action. *Curr. Opin. Biotechnol.* **2007**, *18*, 497−503.
(9) Seaton, A.; Higgins, C.; Mann, J.; Baron, A.; Bailly, C.; Neidle, S.; van den Berg, H. Mechanistic and anti-proliferative studies of two novel, biologically active bis-benzimidazoles. *Eur. J. Cancer* **2003**, *39*, 2548−2555.
(10) Lenglet, G.; David-Cordonnier, M.-H. DNA-destabilizing agents as an alternative approach for targeting DNA: Mechanisms of action and cellular consequences. *J. Nucleic Acids* **2010**, *2010*, 1−17.
(11) Tse, W. C.; Boger, D. L. Sequence-selective DNA recognition: Natural products and nature's lessons. *J. Chem. Biol.* **2004**, *11*, 1607−1617.
(12) Weber, G. F. DNA Damaging Drugs. *Molecular Therapies of Cancer*; Springer: Cham, 2015; pp 9−112.
(13) Bales, B. C.; Kodama, T.; Weledji, Y. N.; Pitié, M.; Meunier, B.; Greenberg, M. M. Mechanistic studies on DNA damage by minor groove binding copper-phenanthroline conjugates. *Nucleic Acids Res.* **2005**, *33*, 5371−5379.
(14) Gupta, S.; Tiwari, N.; Munde, M. A Comprehensive Biophysical Analysis of the Effect of DNA Binding Drugs on Protamine-induced DNA Condensation. *Sci. Rep.* **2019**, *9*, 5891.
(15) Lam, K. S.; Veitch, J. A.; Golik, J.; Krishnan, B.; Klohr, S. E.; Volk, K. J.; Forenza, S.; Doyle, T. W. Biosynthesis of Esperamicin A1, an Enediyne Antitumor Antibiotic. *J. Am. Chem. Soc.* **1993**, *115*, 12340−12345.
(16) Banerjee, D.; Pal, S. K. Dynamics in the DNA recognition by DAPI: Exploration of the various binding modes. *J. Phys. Chem. B* **2008**, *112*, 1016−1021.
(17) Paul, A.; Guo, P.; Boykin, D.; Wilson, W. A new generation of minor-groove-binding—heterocyclic diamidines that recognize G·C base pairs in an at sequence context. *Molecules* **2019**, *24*, 946.
(18) Pjura, P. E.; Grzeskowiak, K.; Dickerson, R. E. Binding of Hoechst 33258 to the minor groove of B-DNA. *J. Mol. Biol.* **1987**, *197*, 257−271.
(19) Drozdowska, D.; Bruzgo, I.; Midura-Nowaczek, K. Carbocyclic potential DNA minor groove binders and their biological evaluation. *J. Enzyme Inhib. Med. Chem.* **2010**, *25*, 629−634.
(20) Fairley, T. A.; Tidwell, R. R.; Donkor, I.; Naiman, N. A.; Ohemeng, K. A.; Lombardy, R. J.; Bentley, J. A.; Cory, M. Structure, DNA minor groove binding, and base pair specificity of alkyl- and aryl-Linked Bis(amidinobenzimidazoles) and Bis(amidinoindoles). *J. Med. Chem.* **1993**, *36*, 1746−1753.
(21) Townsend, L. B.; Wise, D. S. The synthesis and chemistry of certain anthelmintic benzimidazoles. *Parasitol. Today* **1990**, *6*, 107−112.
(22) Merino, G.; Jonker, J. W.; Wagenaar, E.; Pulido, M. M.; Molina, A. J.; Alvarez, A. I.; Schinkel, A. H. Transport of anthelmintic benzimidazole drugs by breast cancer resistance protein (BCRP/ABCG2). *Drug Metab. Dispos.* **2005**, *33*, 614−618.
(23) Agh-Atabay, N.; Dulger, B.; Gucin, F. Synthesis, and investigation of antimicrobial activity of some bisbenzimidazole-derived chelating agents. *Eur. J. Med. Chem.* **2003**, *38*, 875−881.
(24) Arjmand, F.; Mohani, B.; Ahmad, S. Synthesis, antibacterial, antifungal activity and interaction of CT-DNA with a new benzimidazole derived Cu(II) complex. *Eur. J. Med. Chem.* **2005**, *40*, 1103−1110.
(25) Ansari, K. F.; Lal, C. Synthesis, physicochemical properties and antimicrobial activity of some new benzimidazole derivatives. *Eur. J. Med. Chem.* **2009**, *44*, 4028−4033.
(26) Kim, J. S.; Sun, Q.; Yu, C.; Liu, A.; Liu, L. F.; Lavoie, E. J. Quantitative structure-activity relationships on 5-substituted terbnzimidazoles as topoisomerase I poison and antitumor agents. *Bioorg. Med. Chem.* **1998**, *6*, 163−172.
(27) Wang, X.-J.; Chu, N.-Y.; Wang, Q.-H.; Liu, C.; Jiang, C.-g.; Wang, X.-Y.; Ikejima, T.; Cheng, M.-S. Newly synthesized bis-benzimidazole derivatives exerting antitumor activity through induction of apoptosis and autophagy. *Bioorg. Med. Chem. Lett.* **2012**, *22*, 6297−6300.
(28) Fonseca, T.; Gigante, B.; Marques, M. M.; Gilchrist, T. L.; De Clercq, E. Synthesis and antiviral evaluation of benzimidazoles, quinoxalines, and indoles from dehydroabietic acid. *Bioorg. Med. Chem.* **2004**, *12*, 103−112.
(29) Malaty, H.; El-Zimaity, H. M. T.; Genta, R. M.; Cole, R. A.; Graham, D. Y. High-dose proton pump inhibitor plus Amoxycillin for the treatment or retreatment of helicobacter pylori infection. *Aliment. Pharmacol. Ther.* **1996**, *10*, 1001−1004.
(30) Zhang, X.; Kiechle, F. 33342-induced apoptosis is associated with decreased immunoreactive topoisomerase I and topoisomerase I-DNA complex formation. *Ann. Clin. Lab. Sci.* **2001**, *31*, 187−198.
(31) Thomas, A.; Pommier, Y. Targeting Topoisomerase I in the Era of Precision Medicine. *Clin. Cancer Res.* **2019**, *25*, 6581−6589.
(32) Wang, J. C. DNA topoisomerases. *Annu. Rev. Biochem.* **1996**, *65*, 635−692.
(33) Coban, G.; Zencir, S.; Zupkó, I.; Réthy, B.; Gunes, H. S.; Topcu, Z. Synthesis and biological activity evaluation of 1H-benzimidazoles via mammalian DNA topoisomerase I and cytostaticity assays. *Eur. J. Med. Chem.* **2009**, *44*, 2280−2285.
(34) Singh, R.; Pandey, S.; Sur, S.; Tandon, V. PPEF: A bisbenzimdazole potent antimicrobial agent interacts at acidic triad of catalytic domain of E. coli topoisomerase IA. *Biochim. Biophys. Acta, Gen. Subj.* **2019**, *1863*, 1524−1535.
(35) Singh, M.; Tandon, V. Synthesis and biological activity of novel inhibitors of topoisomerase I: 2-Aryl-substituted 2-bis-1H-benzimidazoles. *Eur. J. Med. Chem.* **2011**, *46*, 659−669.
(36) Bansal, S.; Bajaj, P.; Pandey, S.; Tandon, V. Topoisomerases: Resistance versus Sensitivity, How Far We Can Go? *Med. Res. Rev.* **2017**, *37*, 404−438.
(37) Nitiss, J. L. DNA topoisomerase II and its growing repertoire of biological functions. *Nat. Rev. Cancer* **2009**, *9*, 327−337.
(38) Pourqier, P.; Lansiaux, A. Molecular determinants of response to topoisomerase I inhibitors. *Bull. Cancer* **2011**, *98*, 1287−1298.
(39) Tawar, U.; Jain, A. K.; Dwarakanath, B. S.; Chandra, R.; Singh, Y.; Chaudhury, N. K.; Khaitan, D.; Tandon, V. Influence of phenyl ring disubstitution on bisbenzimidazole and terbenzimidazole cytotoxicity: Synthesis and biological evaluation as radioprotectors. *J. Med. Chem.* **2003**, *46*, 3785−3792.
(40) Fudickar, W.; Linker, T. Structural motives controlling the binding affinity of 9,10-bis(methylpyridinium) anthracenes towards DNA. *Bioorg. Med. Chem.* **2020**, *28*, 115432.
(41) Rosu, F.; Gabelica, V.; Houssier, C.; Edwin, De. P. Determination of affinity, stoichiometry, and sequence selectivity of minor groove binder complexes with double-stranded oligodeoxynucleotides by electrospray ionization mass spectrometry. *Nucleic Acids Res.* **2002**, *30*, No. e82.
(42) Bostock-Smith, C. E.; Harris, S. A.; Laughton, C. A.; Searle, M. S. Induced fit DNA recognition by a minor groove binding analogue of Hoechst 33258: Fluctuations in DNA A tract structure investigated by NMR and molecular dynamics simulations. *Nucleic Acids Res.* **2001**, *29*, 693−702.
(43) Ranjan, N.; Kellish, P.; King, A.; Arya, D. P. Impact of Linker Length and Composition on Fragment Binding and Cell Permeation:

https://doi.org/10.1021/acsomega.1c05743
ACS Omega 2022, 7, 2861−2880

Story of a Bisbenzimidazole Dye Fragment. *Biochemistry* **2017**, *56*, 6434−6447.
(44) Amirbekyan, K.; Duchemin, N.; Benedetti, E.; Joseph, R.; Colon, A.; Markarian, S. A.; Bethge, L.; Vonhoff, S.; Klussmann, S.; Cossy, J.; et al. Design, Synthesis, and Binding Affinity Evaluation of Hoechst 33258 Derivatives for the Development of Sequence-Specific DNA-Based Asymmetric Catalysts. *ACS Catal.* **2016**, *6*, 3096−3105.
(45) Shoemaker, R. H. The NCI60 human tumour cell line anticancer drug screen. *Nat. Rev. Cancer* **2006**, *6*, 813−823.
(46) Selwood, D. Anticancer Drug Development: Preclinical Screening, Clinical Trials, and Approval. *Br. J. Cancer* **2004**, *91*, 1000.
(47) Shaharyar, M.; Abdullah, M. M.; Bakht, M. A.; Majeed, J. Pyrazoline bearing benzimidazoles: Search for anticancer agent. *Eur. J. Med. Chem.* **2010**, *45*, 114−119.
(48) Rashid, M.; Husain, A.; Mishra, R. Synthesis of benzimidazoles bearing oxadiazole nucleus as anticancer agents. *Eur. J. Med. Chem.* **2012**, *54*, 855−866.
(49) Paul, K.; Sharma, A.; Luxami, V. Synthesis and in vitro antitumor evaluation of primary amine substituted quinazoline linked benzimidazole. *Bioorg. Med. Chem. Lett.* **2014**, *24*, 624−629.
(50) Hearn, J. M.; Romero-Canelón, I.; Qamar, B.; Liu, Z.; Hands-Portman, I.; Sadler, P. J. Organometallic Iridium(III) anticancer complexes with new mechanisms of action: NCI-60 screening, mitochondrial targeting, and apoptosis. *ACS Chem. Biol.* **2013**, *8*, 1335−1343.
(51) Phillips, M. A. CCCXVII. The formation of 2-substituted benziminazoles. *J. Chem. Soc.* **1928**, 2393−2399.
(52) Singh, M. P.; Sasmal, S.; Lu, W.; Chatterjee, M. N. Synthetic utility of catalytic Fe(III)/Fe(II) redox cycling towards fused heterocycles: A facile access to substituted benzimidazole, bisbenzimidazole, and imidazopyridine derivatives. *Synthesis* **2000**, 1380−1390.
(53) Wright, J. B. The Chemistry of the Benzimidazoles. *Chem. Rev.* **1951**, *48*, 397−541.
(54) Bahrami, K.; Khodaei, M.; Kavianinia, I. A simple and efficient one-pot synthesis of 2-substituted benzimidazoles. *Synthesis* **2007**, 547−550.
(55) Shen, M.; Driver, T. G. Iron (II) bromide-catalyzed synthesis of benzimidazoles from aryl azides. *Org. Lett.* **2008**, *10*, 3367−3370.
(56) Hegedüs, A.; Hell, Z.; Potor, A. Zeolite-catalyzed environmentally friendly synthesis of benzimidazole derivatives. *Synth. Commun.* **2006**, *36*, 3625−3630.
(57) Curini, M.; Epifano, F.; Montanari, F.; Rosati, O.; Taccone, S. Ytterbium triflate promoted synthesis of benzimidazole derivatives. *Synlett* **2004**, 1832−1834.
(58) Deng, X.; McAllister, H.; Mani, N. S. CuI-catalyzed amination of arylhalides with guanidines or amidines: A facile synthesis of 1-H-2-substituted benzimidazoles. *J. Org. Chem.* **2009**, *74*, 5742−5745.
(59) Nimesh, H.; Sur, S.; Sinha, D.; Yadav, P.; Anand, P.; Bajaj, P.; Virdi, J. S.; Tandon, V. Synthesis and Biological Evaluation of Novel Bisbenzimidazoles as Escherichia coli Topoisomerase IA Inhibitors and Potential Antibacterial Agents. *J. Med. Chem.* **2014**, *57*, 5238−5257.
(60) Redinbo, M. R.; Champoux, J. J.; Hol, W. G. J. Novel Insights into Catalytic Mechanism from a Crystal Structure of Human Topoisomerase I in Complex with DNA. *Biochemistry* **2000**, *39*, 6832−6840.
(61) Friesner, R. A.; Murphy, R. B.; Repasky, M. P.; Frye, L. L.; Greenwood, J. R.; Halgren, T. A.; Sanschagrin, P. C.; Mainz, D. T. Xtra Precision Glide:Docking and Scoring incorporating a model of hydrophobic enclosure for Protein−Ligand Complexes. *J. Med. Chem.* **2006**, *49*, 6177−6196.
(62) Halgren, T. A.; Murphy, R. B.; Friesner, R. A.; Beard, H. S.; Frye, L. L.; Pollard, W. T.; Banks, J. L. Glide: a new approach for rapid, accurate docking and scoring. 2. Enrichment factors in database screening. *J. Med. Chem.* **2004**, *47*, 1750−1759.
(63) Bart, L.; Hjerrild, K.; Feese, M. D.; Behnke, C. A.; Burgin, A. B.; Stewart, L. The mechanism of topoisomerase I poisoning by a camptothecin analog. *Proc. Natl. Acad. Sci. U.S.A.* **2002**, *99*, 15387−15392.
(64) Laskowski, R. A.; Swindells, M. B. LigPlot+: multiple ligand-protein interaction diagrams for drug discovery. *J. Chem. Inf. Model.* **2011**, *51*, 2778−2786.
(65) Biovia. Dassault Systèmes. *Discovery Studio Visualizer*: San Diego, CA, USA, 936, 2017.
(66) Carrondo, M. A. A. F. d. C. T.; Coll, M.; Aymami, J.; Wang, A. H. J.; Van der Marel, G. A.; Van Boom, J. H.; Rich, A. Binding of a Hoechst Dye to d(CGCGATATCGCG) and Its Influence on the Conformation of the DNA Fragment. *Biochemistry* **1989**, *28*, 7849−7859.
(67) Quintana, J. R.; Lipanov, A. A.; Dickerson, R. E. Low-Temperature Crystallographic Analyses of the Binding of Hoechst 33258 to the Double-Helical DNA Dodecamer C-G-C-G-A-A-T-T-C-G-C-G. *Biochemistry* **1991**, *30*, 10294−10306.
(68) Guo, P.; Farahat, A. A.; Paul, A.; Harika, N. K.; Boykin, D. W.; Wilson, W. D. Compound Shape Effects in Minor Groove Binding Affinity and Specificity for Mixed Sequence DNA. *J. Am. Chem. Soc.* **2018**, *140*, 14761−14769.
(69) Han, F.; Taulier, N.; Chalikian, T. V. Association of the minor groove binding drug Hoechst 33258 with d(CGCGAATTCGCG)2: Volumetric, calorimetric, and spectroscopic characterizations. *Biochemistry* **2005**, *44*, 9785−9794.
(70) Singh, M.; Sur, S.; Rastogi, G. K.; Jayaram, B.; Tandon, V. Bi and tri-substituted phenyl rings containing bisbenzimidazoles bind differentially with DNA duplexes: A biophysical and molecular simulation study. *Mol. BioSyst.* **2013**, *9*, 2541−2553.
(71) Boyd, M. R.; Paull, K. D. Some Practical Considerations and Applications of the National Cancer Institute In Vitro Anticancer Drug Discovery Screen. *Drug Dev. Res.* **1995**, *34*, 91−109.
(72) Skehan, P.; Storeng, R.; Scudiero, D.; Monks, A.; McMahon, J.; Vistica, D.; Warren, J. T.; Bokesch, H.; Kenney, S.; Boyd, M. R. New colorimetric cytotoxicity assay for anticancer-drug screening. *J. Natl. Cancer Inst.* **1990**, *82*, 1107−1112.
(73) Chabner, B. A. NCI-60 Cell Line Screening: A Radical Departure in Its Time. *J. Natl. Cancer Inst.* **2016**, *108*, djv388.
(74) Staker, B. L.; Hjerrild, K.; Feese, M. D.; Behnke, C. A.; Burgin, A. B.; Stewart, L. The mechanism of topoisomerase I poisoning by a camptothecin analog. *Proc. Natl. Acad. Sci. U.S.A.* **2002**, *99*, 15387−15392.
(75) Pommier, Y. Topoisomerase I inhibitors: camptothecins and beyond. *Nat. Rev. Cancer* **2006**, *6*, 789−802.
(76) Jian-Song, J.; Gao, Q.-L.; Wu, B.-W.; Li, D.; Shi, L.; Zhu, T.; Lou, J.-F.; Jin, C.-Y.; Zhang, Y.-B.; Zhang, S.-Y.; Liu, H.-M. Novel tertiary sulfonamide derivatives containing benzimidazole moiety as potent anti-gastric cancer agents: Design, synthesis, and SAR. *Eur. J. Med. Chem.* **2019**, *183*, 111731.

https://doi.org/10.1021/acsomega.1c05743
ACS Omega 2022, 7, 2861−2880